Alma Mater Studiorum · Università di Bologna

Scuola di ingegneria e architettura · Cesena

Corso di Laurea Magistrale in
Ingegneria elettronica e telecomunicazioni per l'energia

REAL-TIME CONTROL OF AN ELECTRODYNAMIC SHAKER

Tesi Di Laurea Magistrale In
Elettronica dei sistemi digitali

Relatore:
Prof. Ing.
ALDO ROMANI

Presentata da:
LUCA MARTINI

Correlatori:
Dr.-Ing.
Loreto Mateu

Dr.-Ing.
Henrik Zessin

II Appello - III Sessione
Anno Accademico 2014/2015

This page intentionally left blank.

Keywords:

Electrodynamic Shaker

Control Loop

Inverse Modeling

Adaptive Filtering Algorithm

This page intentionally left blank.

Ringraziamenti:

I miei più sinceri ringraziamenti vanno al Prof. Ing. Aldo Romani, per il supporto, la disponibilità e i consigli che mi ha fornito in questo periodo di tesi all'estero.

Vorrei inoltre ringraziere i miei correlatori Dr.-Ing. Loreto Mateu e Dr.-Ing. Henrik Zessin che hanno seguito il mio lavoro nel periodo di permanza al Fraunhofer IIS institute.

Uno speciale ringraziamento va ai colleghi che ho conosciuto all'interno dell'istituto e che hanno reso veramente piacevole ed indimenticabile questa esperienza.

Alla mia famiglia e amici va inoltre uno speciale ringraziemento per aver reso possibile questa esperienza, grazie.

Sommario:

Il consumo energetico di circuiti e sistemi microelettronici è progressivamente diminuito con l'evoluzione della tecnologia dei semiconduttori. Per questa ragione il tema dell'*energy harvesting* è sempre più considerato un punto chiave nello sviluppo di sistemi autonomi e microsistemi ad esteso tempo di vita. I trasduttori meccanici di energia sono in grado utilizzare l'energia presente nell'ambiente per alimentare piccoli dispositivi elettronici come sensori, microcontrollori e nodi wireless. Questa tecnologia viene correntemente denominata *energy harvesting*, inoltre, i sistemi alimentati con questi generatori sono spesso chiamati *energy-autarkic* o auto-alimentati.
Le ricerche nel campo dell'energy harversting si basano sul concetto fondamentale di convertire semplici vibrazioni armoniche in energia elettrica. Negli ultimi anni la ricerca si è orientata sulla conversione di svariate forme di energia meccanica, come quella impulsiva derivante dal cammino delle persone, dalle vibrazioni random ambientali, dalle deformazioni superficiali di strutture civili o dalle sollecitazioni meccaniche dovute a flussi di aria o liquidi.
Questa tesi è essenzialmente focalizzata sullo sviluppo di un sistema di controllo in tempo reale per uno shaker elettrodinamico usato per riprodurre profili di vibrazione ambientale registrati in contesti reali e di interesse per il recupero di enrgia. Grazie all'utilizzo di uno shaker elettrodinamico è quindi possibile riprodurre scenari di vibrazione reale in laboratorio e valutare più agevolmente le prestazioni dei trasduttori meccanici. Differenti tipi di shaker vengono utilizzati in test di vibrazione (idraulici, pneumatici, piezoelettrici, elettrodinamici, rotativi), ma per lo studio di vibrazioni ambientali gli shaker elettrodinamici sono nella maggioranza dei casi la scelta migliore, grazie all'elevato rage dinamico, larghezza di banda e flessibilità di utilizzo. Tuttavia, è richiesto un controllo dello shaker non solo in termini di stabilità ma anche per garantire l'esatta riproduzione del segnale registrato nel contesto reale. In questa tesi, si è scelto di sviluppare un controllo adattivo nel dominio del tempo per garantire la corretta riproduzione del profilo di accelerazione desiderato. L'algoritmo è stato poi implementato sul sistema di prototipazione rapida dSPACE DS1104 basata su microprocessore PowerPC. La natura adattiva dell'algoritmo proposto permette di identificare cambiamenti nella risposta dinamica del sistema, e di regolare di conseguenza i parametri del controllore. Il controllo del sistema è stato ottenuto anteponendo al sistema un filtro adattivo la cui funzione di trasferimento viene continuamente adattata per rappresentare al meglio la funzione di trasferimento inversa del sistema da controllare. Esperimenti in laboratorio confermano l'efficacia del controllo nella riproduzione di segnali reali e in tipici test di *sweep* frequenziale.

Abstract:

In the last years, the energy request of micro-electronic systems is decreasing because of the successive improvement in the semiconductors technology. Accordingly, the topic of energy harvesting is considered an interesting opportunity in the development of autonomous microsystems with extended lifetimes. [1, 2]. Mechanical transducers are able to convert ambient energy to power small electronic devices such as sensors, microcontrollers, and wireless transceiver.
Mechanical energy harvesting started with the simple idea of converting vibrations into electricity.
In the last years, particular interest is reserved at the conversion of common type of mechanical energy, such as vibration energy from human gait, environmental vibrations and acoustic energy of waves. [3]
This thesis is essentially focused on an adaptive vibration control system for an electrodynamic shaker, in order to reproduce the same vibration profile recorded at the location of interest in the real environment. In this way, realistic scenarios can be reproduced in the laboratory.
There are several types of vibrational exciters (ok shakers) used in vibration tests, but for the reproduction of real environment conditions, the electrodynamic exciters are usually the best solution, due to their high dynamic range, frequency range and compactness. The control of the shaker is required to provide a good replication of the given reference signal and stable control [4]. In this thesis, a time domain adaptive filtering algorithm for control the acceleration applied on the specimen is developed. The algorithm was implemented using dSPACE DS1104 PowerPC. The proposed algorithm permit to identifies changes in system and update the parameters of the controller accordingly.
Preceding the system that has to be controlled with an adaptive filter whose frequency response is the inverse of the frequency response of the system, permit to achieve the control of the system dynamics.
Real experiments are performed for sine sweep (sine-dwell) and real vibration replication tests [44].

This page intentionally left blank.

Contents

Chapter 1

Introduction

1.1 Structure of thesis

The thesis is presented in five chapters. The first chapter contains background informations on vibration testing using the electrodynamic shaker. The chapter also discusses the fundamentals signal used in energy harvesting vibration test and the basic knowledge about adaptive filter and inverse modelling.
In the second chapter the vibration test equipment is discussed. Mathematical analysis and the model of the shaker system are derived. The swept sine test method is used to characterise the open loop dynamics of the shaker system.
In third chapter the time domain adaptive inverse model control are used. A performance behaviour is presented and the computational complexity , convergence rate and and memory requirements are discussed.
In fourth chapter the adaptive control algorithm is implemented and used to control the shaker/specimen system.
The final chapter contains conclusion and future development.

1.2 Background

1.2.1 Electrodynamic shaker fundamentals

The structure of an electrodynamic exciter call to mind the structure of a loudspeaker, but it is heavier and more robust (Figure. 1.1).

Figure. 1.1a shows a sketch illustrating the basic design of a shaker. It consists of a permanent magnet which produces the required constant magnetic field, a coil which is fed from an AC signal source, an armature (on which the coil is mounted), and a flexure. The flexures hold the coil and moving elements in position with respect to the constant magnetic field. The armature coil is suspended in a fixed

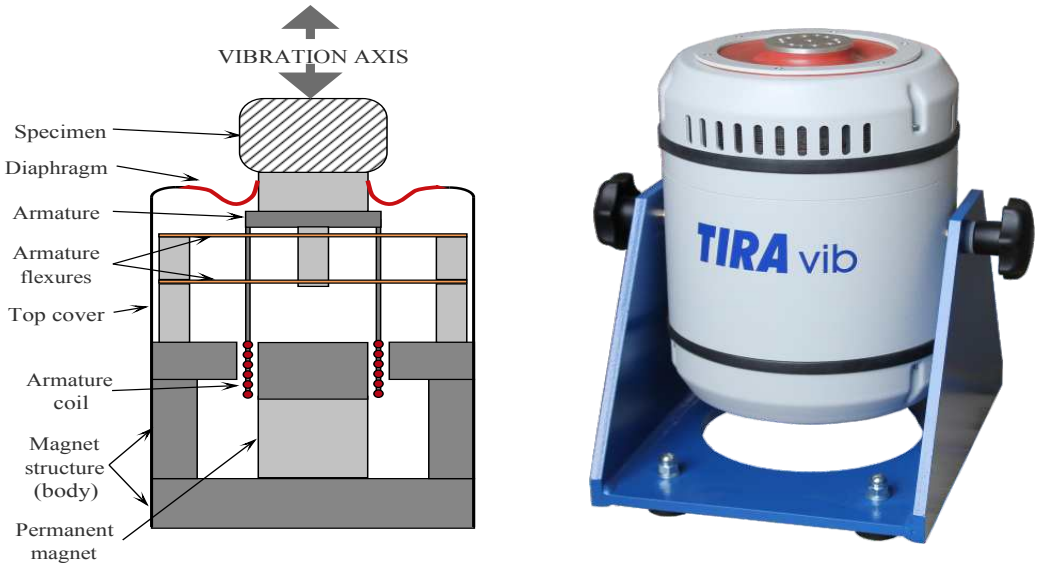

(a) Electrodynamic shaker cross-section (b) TIRA S52110 vibration exciter [5]

Figure 1.1: The structure of an electrodynamic shaker

radial magnetic field, when a current flows in the coil, an axial force proportional to the current and the magnetic flux intensity is produced, according to the Lorentz force (Eq.1.1).

$$f_{em} = B\ell i_a = \Gamma i_a \tag{1.1}$$

f_{em} : is the force [N]
i_a : is the current flow [A]
ℓ : is the length of the coil wire in the field [m]
B : is the magnetic field [T]
Γ : the shaker ratio of thrust to coil current $\Gamma = B\ell$ [N/A]

This force is transmitted to a table structure to which the test article may be fixed. The magnetic flux cutting the coil, number of turns within the flux and the current, determine the force available. This force is limited by the cooling provided for the coil, the saturation current, the materials, and by the mechanical strength of the moving parts. In general the shaker coil resistance is lower than that of a normal loudspeaker, which is a key-factor in the selection of a companion power amplifier. The coil impedance is complex and the minimum impedance value at the shaker input terminal is the DC resistance. The coil impedance increases proportionally with frequency. As well the coupling interaction between electrical and mechanical domain generate a voltage in proportion to the coil velocity (Eq. 1.2) (Eq. 1.3).

$$v_a = Ri_a + L\frac{di_a}{dt} + e \tag{1.2}$$

$$e = \Gamma\frac{dx_c}{dt} \tag{1.3}$$

v_a : is the voltage at the armature terminals [V]
R : is the coil resistance [Ohm]
L : is the coil inductance [H]
$\frac{dx_c}{dt}$: is the armature velocity [m/s]
e : is the back electromotive force [V]

This back electro-magnetic field is reflected in the electrical domain via an increase in the coil impedance [6, 7].
A typical resonance characteristic of vibration exciters, when the input current (thus the force) to the drive coil is kept constant and independent of frequency, is shown in Figure. 1.2 [8]. In this case, only the structural damping can be seen, due to the fact that shaker's response affects the output voltage, but the current level is fixed by the power amplifier and independent of the generated back electromagnetic field.

At very low frequency the displacement of the moving elements is defined by the stiffness of the armature flexures, i.e., constant displacements at the shaker table, region A (Figure. 1.2).
When the frequency of the driving signal is increased, the one degree-of-freedom, spring/mass/damper vibration system, cause a relatively great increase in the table's acceleration, region B (Figure. 1.2). Here, the coil and the armature move together, relative to the shaker body. For increasing frequencies, the suspension resonance is negligible, and a region of constant acceleration is developed, region C (Figure. 1.2). At or beyond the high frequency limit of operation, the moving elements itself will resonate. Here, the coil moves out of phase with the armature structure, which is therefore deformed, region D (Figure. 1.2). Excessive excitation of this mode can damage the shaker, as well this resonance limits the upper end of the useful frequency range [6]. Figure. 1.3 shows the frequency response of the current-driven electromagnetic shaker used in this thesis.

The frequency response of an electrodynamic shaker can also be evaluated in a voltage-driven mode, in this case the power amplifier imposes a voltage to the armature's coil, and the frequency response reflects the very significant electromagnetic damping caused by the cross-coupling terms between the electrical and mechanical components of the system (Eq. 1.3) [6, 7]. Figure. 1.4 shows the frequency response of the voltage-driven electromagnetic shaker used in this thesis.

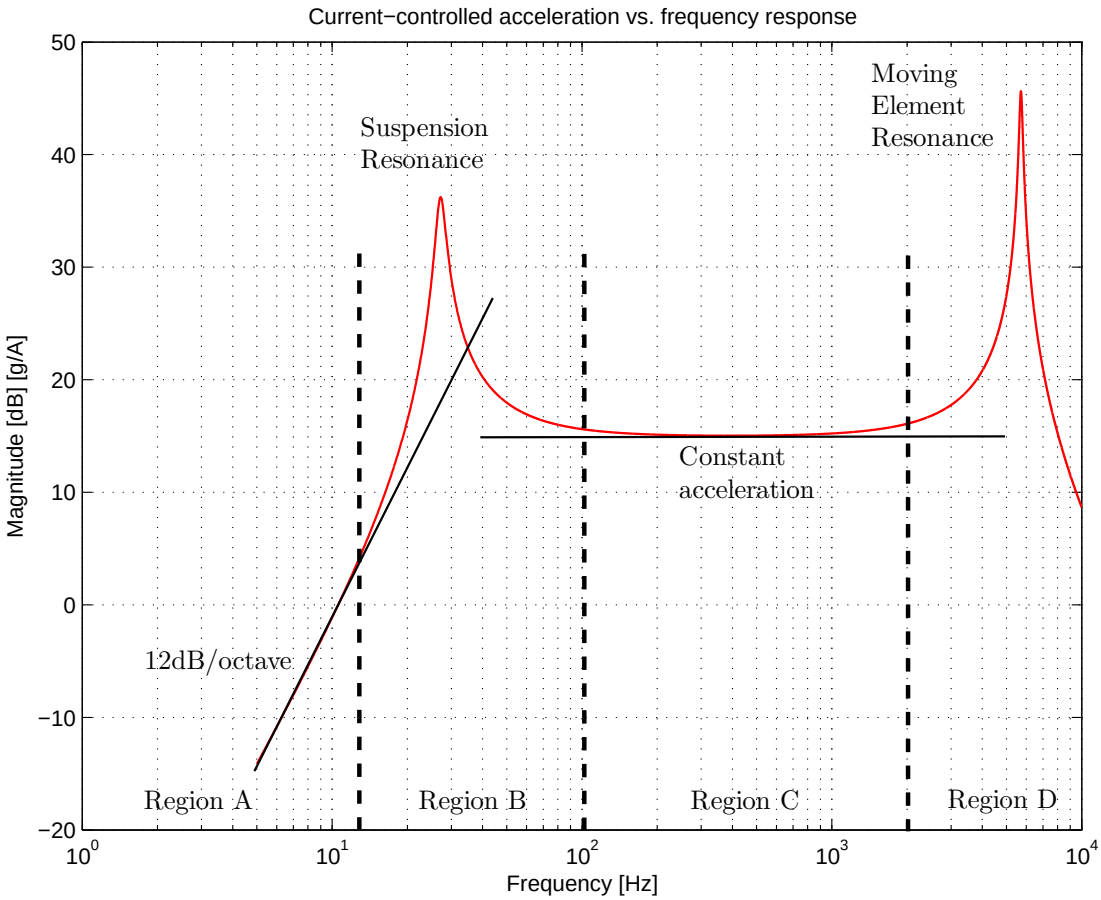

Figure 1.2: current-controlled acceleration vs. frequency response of vibration exciters [8]

Ideally the coil and moving element should be a rigid unit where all points move in phase in one-dimensional movement, and the loading of the shaker should in no way influence the table motion. Unfortunately, it is not possible satisfy this ideal conditions and a compromise is necessary. To achieve pure one-dimensional motion, the specimen must be constrained in such a way that no other modes of movement is possible [8, 9]. To contain the effect of the specimen resonances on the moving element, a certain acceleration of the specimen a rather high force is needed, for example this can be achieved by increasing the mass of the moving element. Furthermore, adding a mass on the moving element normally reduces the useful frequency range of the shaker. By introducing a control-loop for the moving elements motion it is possible to minimize the influence of the load. Then smaller masses can be used for the same test, and a much greater part of the force

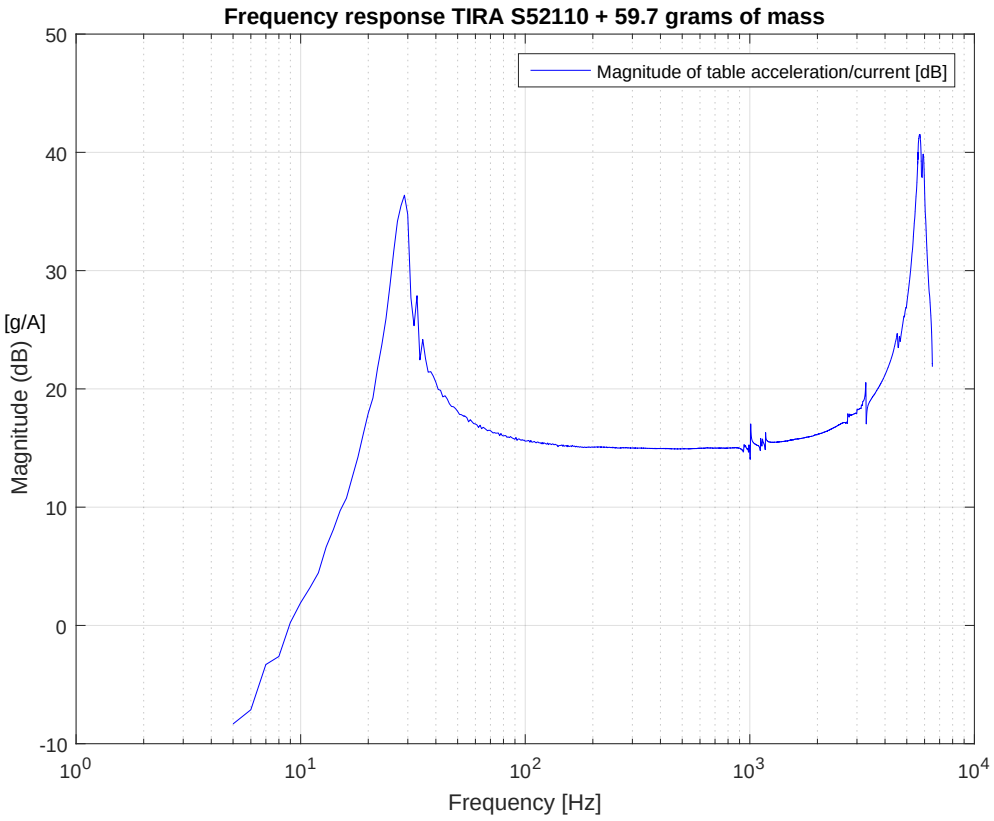

Figure 1.3: current-driven frequency response of TIRA S52110 electrodynamic shaker plus 59.7 grams of mass

produced by the shaker is transferred to the specimen.

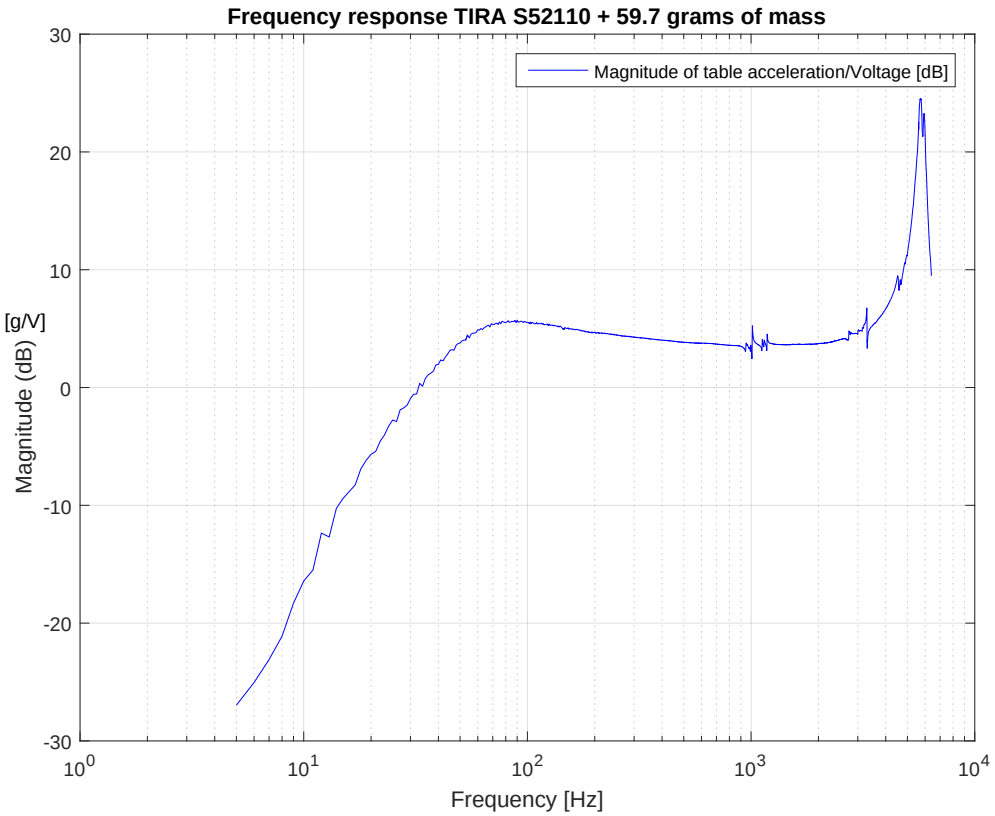

Figure 1.4: voltage-driven frequency response of TIRA S52110 electrodynamic shaker plus 59.7 g of mass

1.2.2 Adaptive filter

In the context of signals and systems, the term *filter* is commonly used to refer to a system that changes the harmonic content of the incoming signal in order to provide an output signal with some desirable characteristics.
Adaptive filters are often realized either as a set of program instructions running on a digital signal processor (DSP), or as a set of logic operations implemented in a field-programmable gate array (FPGA).
In this thesis, only discrete-time signal and digital linear filters are considered. Accordingly, all the signals are represented in therms of sequences. The internal structure of a linear discrete-time filter is completely characterized by its impulse response, or by its transfer function in the frequency domain.
The adjective *adaptive* refers to a system that is trying to modify its transfer function with the aim of achieve some well-defined goal that is function of the state of the system or on its surroundings (Figure. 1.5).

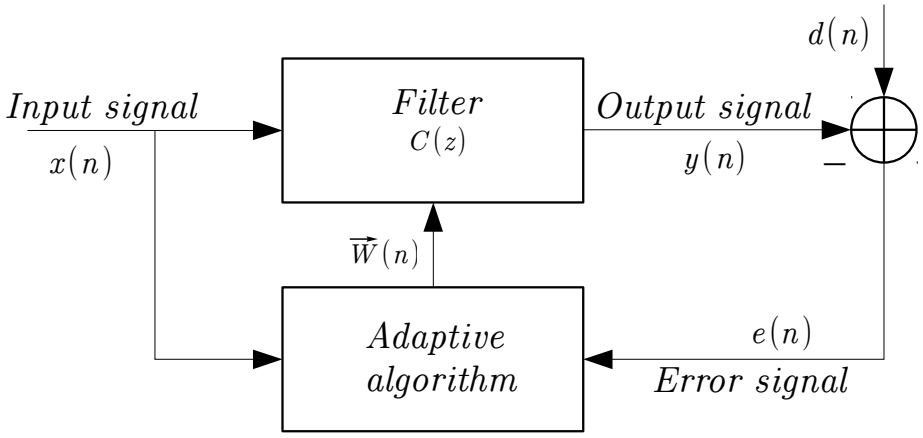

Figure 1.5: Schematic diagram of an adaptive filter

In an adaptive system, the filter is employed to modify the frequency content of the input signal in order to generate a good estimation of the given desired signal. The filter coefficients are adapted in order to achieve the best match between the filter output and the desired signal. This process usually consist in the optimization of a defined cost function, and it can be determined in a statistical or deterministic approach [10].
The general operating principle of the algorithm that is used in this thesis, is to

correlate the error of the filter with the samples of the filter input, and update the filter parameters by a recursive equation that use this result. The main reasons to implement the adaptive filter iteratively are as follows [10]:

- A large amount of signal samples are required for the direct calculation of the filter coefficients, i.e. a significant amount of resource are needed in terms of memory. Iterative implementations do not require the storing of samples, therefore advantage in term of memory.

- A large delay is introduced when the collection of samples and their post-processing is required to generate the output signal (as required in non-iterative solutions). This is unsuitable for many real-time applications, e.g., the real-time control of an electrodynamic shaker discussed in this thesis. Vice versa, no significant delay is introduced in iterative implementation, and a real time control can be addressed.

- Iterative implementation presents some tracking capability. If the harmonic content of the signal, or the transfer function of the system that we want to control change are time dependent, an iterative updating of the filter will be able to follow the new property of the system.

- Implementing in code or hardware an iterative solution is usually more simpler than a non-iterative equivalent solution.

The most commons adaptive filter structures uses a finite impulse response (FIR) or infinite impulse response (IIR) filter to define the relationship between the desired and the input signals.

However, the adaption process of an IIR filter involves many complication, and their application is rather limited in the adaptive filter solutions [11, 12]. Especially, during the adaption process they can easily become unstable because of their poles may be moved outside the the unit circle in the z-plane. Moreover, the general IIR performance function has not only one global minimum point but many local minima. This may cause the convergence to one of the local minima and not in the best solution [10, 11, 13]. Vice versa, the mean squared error (MSE) formulation of FIR filters and linear combiners are well-defined in a quadratic function with a single minimum point. [10].

1.2.3 Adaptive inverse modelling process

In the tracking application, the inverse of the physical system can be used as a controller when the inverse model is cascaded with the physical system to control, as explained in the chapter 3.2.

Pursuing this idea, the next step is finding the inverse of the system that needs to be controlled. In Figure. 1.6 $H(z)$ represents the system transfer function. The system inverse, to be used as controller, is represented by $C(z)$ if it is ideal, or by $\hat{C}(z)$ if it is an estimation of the ideal inverse system.

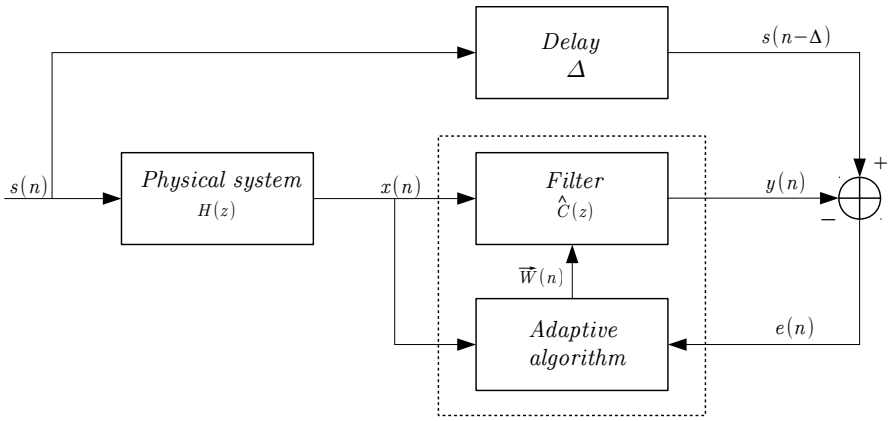

Figure 1.6: Block diagram of the general adaptive inverse system identification problem (inverse modeling or deconvolution).

As stated previously, cascading the adaptive filter with the physical system causes the adaptive filter to converge to a solution that is the inverse of the physical system. The input signal $s(n)$ is filtered through a physical system, the output signal $x(n)$ is processed by the adaptive inverse estimator of the physical system $\hat{C}(z)$. The coefficients of the FIR filter are iteratively adjusted with the aim to minimize the the error signal $e(n)$. The error signal is defined as $e(n) = s(n - \Delta) - y(n)$ were $s(n - \Delta)$ is the delayed copy of the input signal $s(n)$.
Ideally, when the error signal is zero, the convolution of the inverse system estimator impulse response and the physical system imppulse response produce a single impulse $\delta(n)$ delayed of Δ samples $\delta(n - \Delta)$.
In other words, the error signal $e(n)$ reaches its minimum when the product of the filter frequency response $C(z)$ and the physical system frequency response $H(z)$ is unity gain (Eq. 1.4).

$$H(z)C(z) = 1 \tag{1.4}$$

Suppose now that $H(z)$ is minimum-phase, a perfect inverse $C(z)$ exist and would be both stable and causal. This leads to equation 1.5.

$$C(z) = \frac{1}{H(z)} \tag{1.5}$$

Nevertheless, the inverse of a non-minimum phase system would have poles outside the unit circle on the z-plane, and the stability of the inverse model should be considered. In control theory and signal processing, a linear, time-invariant system is said to be minimum-phase if the system and its inverse are causal and stable [14].

However, the causality and stability conditions are satisfied only if all poles of a rational transfer function lies inside the the unit circle on the complex plane.

Assuming that a discrete, rational transfer function has poles and zeros, a perfect inverse of this transfer function presents zeros in the original poles positions, and poles in the original zeros position. As a consequence, that rational transfer function satisfy the minimum-phase requirements only if all its zeros and all its poles are inside the unit circle.
Suppose that the transfer function $H(z)$ can be factorised as (Eq. 1.6):

$$H(z) = z^{-K}\frac{N(z^{-1})}{D(z^{-1})} \tag{1.6}$$

where $N(z^{-1})$ and $D(z^{-1})$ are polynomial functions of z^{-1}. If all roots of $N(z^{-1})$ are inside the unit circle, then the system inverse corresponds to a causal and stable inverse system (Eq. 1.7).

$$C(z) = \frac{D(z^{-1})}{N(z^{-1})} \tag{1.7}$$

The optimal FIR model would be the first M terms of the impulse response of $C(z)$(Eq. 1.8) [15].

$$\hat{C}(z) = \hat{c}_0 + \hat{c}_{-1}z^{-1} + \hat{c}_{-2}z^{-2} + \cdots + \hat{c}_{-M+1}z^{-M+1} \tag{1.8}$$

where M is the length of the FIR filter.

In the real application it is not always possible to know if the system satisfy the minimum-phase requirements. However, in practice implementation this uncertainty can be overcome by introducing delay in the modeling process.

According with the two-side Laplace transforms, a two sided stable inverse would exist for all linear time-invariant systems. Furthermore,it is possible to expand the inverse of a non-minimum phase stable system in a noncausal but stable series. Obviously a causal FIR filter $\hat{C}(z)$ could not represent a noncausal transfer function, but it could be used to approximate a delayed version of the two sided system inverse. In this case the adaptive FIR filter can self-adjust to this function. A much larger delay Δ allows to involve more noncausal terms of the series expansion in the filter transfer function $\hat{C}(z)$, and a better delayed inverse would be the result. With an infinite delay Δ the delayed inverse results perfect, however it is useless from a practical point of view. The choice of Δ is generally

not critical. If no informations about the system are available, Δ could be set equal to the half of the FIR filter length. [16–18].

Consider as an example a non-minimum phase physical system represented by the time-discrete transfer function (Eq. 1.9):

$$H(z) = \frac{1}{10} \cdot \frac{1 + \frac{7}{3}z^{-1} + \frac{2}{3}z^{-2}}{1 - \frac{11}{20}z^{-1} + \frac{1}{5}z^{-2}} \tag{1.9}$$

with its related impulse response (Figure. 1.7).

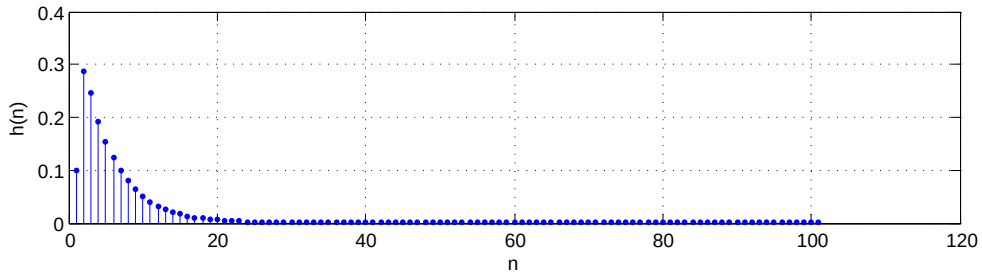

Figure 1.7: Impulse response of $H(z)$

This system is causal and stable, but non-minimum phase, because its zero lies outside the unit circle in the z-plane (Figure. 1.8).

The inverse of this plant can be calculated as (Eq. 1.10):

$$C(z) = \frac{1}{H(z)} = 10 \cdot \frac{z^2 + \frac{11}{20}z - \frac{1}{5}}{z^2 + \frac{7}{3}z - \frac{2}{3}} \tag{1.10}$$

The time-discrete transfer function $C(z)$ is unstable, since is pole is outside the unit circle (Figure. 1.10). The corresponding causal expansion of (Eq. 1.10) is (Eq. 1.11) [19].

$$c(n) = 14.7(-2)^n u(n) - 1.7(-1/3)^n u(n) - 3\delta(n) \tag{1.11}$$

Consider the first term of the causal expansion $14.7(-2)^n u(n)$, its unstable, and grows without bound (Figure. 1.9).

In order to obtain a stable form for the first term, we need to consider the correspondents noncausal, but stable, inverse $-14.7(-2)^n u(-n-1)$. Therefore, to obtain a stable system, the impulse response must be given by (Eq. 1.12).

$$c(n) = -14.7(-2)^n u(-n-1) - 1.7(-1/3)^n u(n) - 3\delta(n) \tag{1.12}$$

The impulse response of $c(n)$ is shown in Figure. 1.11.

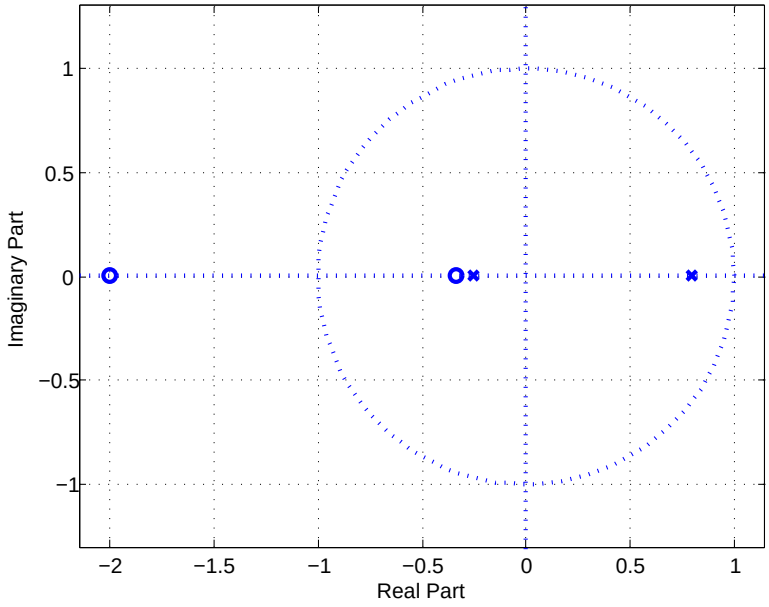

Figure 1.8: poles and zeros of $H(z)$

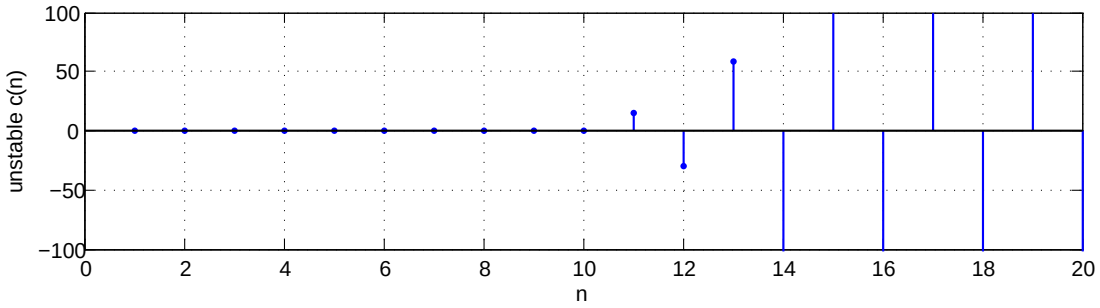

Figure 1.9: impulse response of a causal inverse of $H(z)$

As previously said, $c(n)$ is noncausal and therefore not realizable by the FIR. As long as we consider the series for $n < -10$, the values of $c(n)$ are negligible, and for practical purposes can be set to zero. Setting this terms to zero allows the consideration of the shifted signal:

$$\hat{c}(n) = \begin{cases} c(n-\Delta), & \text{if } n \geq 0 \\ 0, & \text{if } n < 0 \end{cases}$$

with $\Delta = 10$, as a causal and implementable impulse response (Figure. 1.12).

To evaluate the inverse system, we can verify the numerical convolution $h(n) * \hat{c}(n)$.

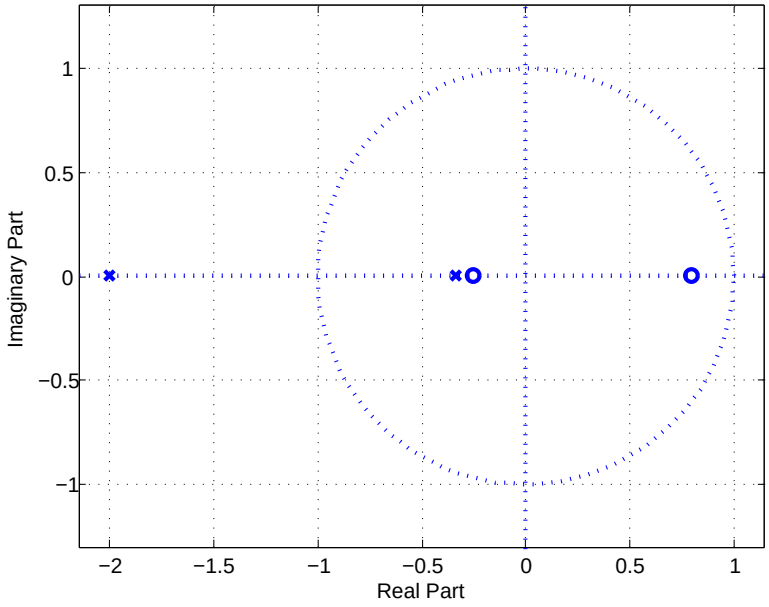

Figure 1.10: poles and zeros of $C(z)$

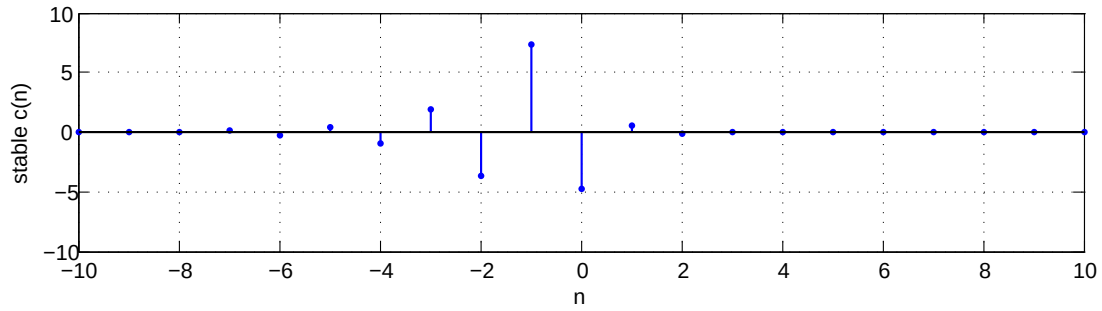

Figure 1.11: impulse response of a noncausal inverse of $H(z)$

For a optimum inverse system, it is required that the convolution $h(n) * c(n) = \delta(n)$. Meanwhile, for a delayed inverse, the convolution $h(n) * \hat{c}(n) = \delta(n - \Delta)$ (Figure. 1.13).

An infinitely long adaptive filter could perfectly emulate $C(z)$. However, infinitely long impulse response is not possible to implement, but a sufficient long one can make the difference between $\hat{C}(z)$ and $C(z)$ negligible.

The adaptive process illustrated in Figure. 1.6 for finding a system inverse, is based on the pre-assumption of the physical system stability. If the system is itself unstable, is necessary to stabilize it via a dedicate internal feedback loop, and then the adaptive inverse estimator can be applied to the stable system [18]. However,

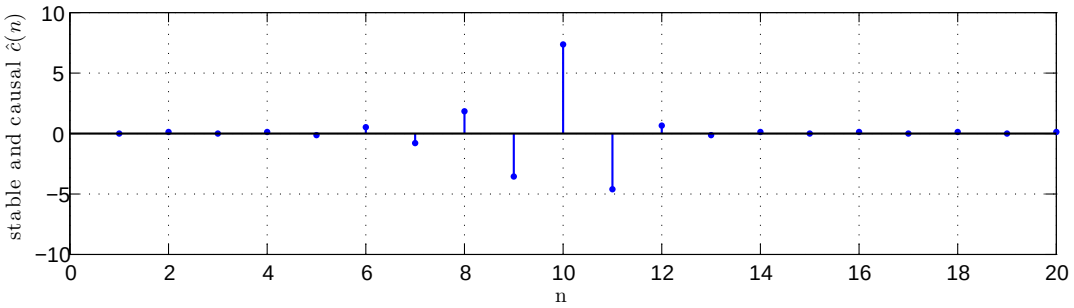

Figure 1.12: Stable and causal impulse response

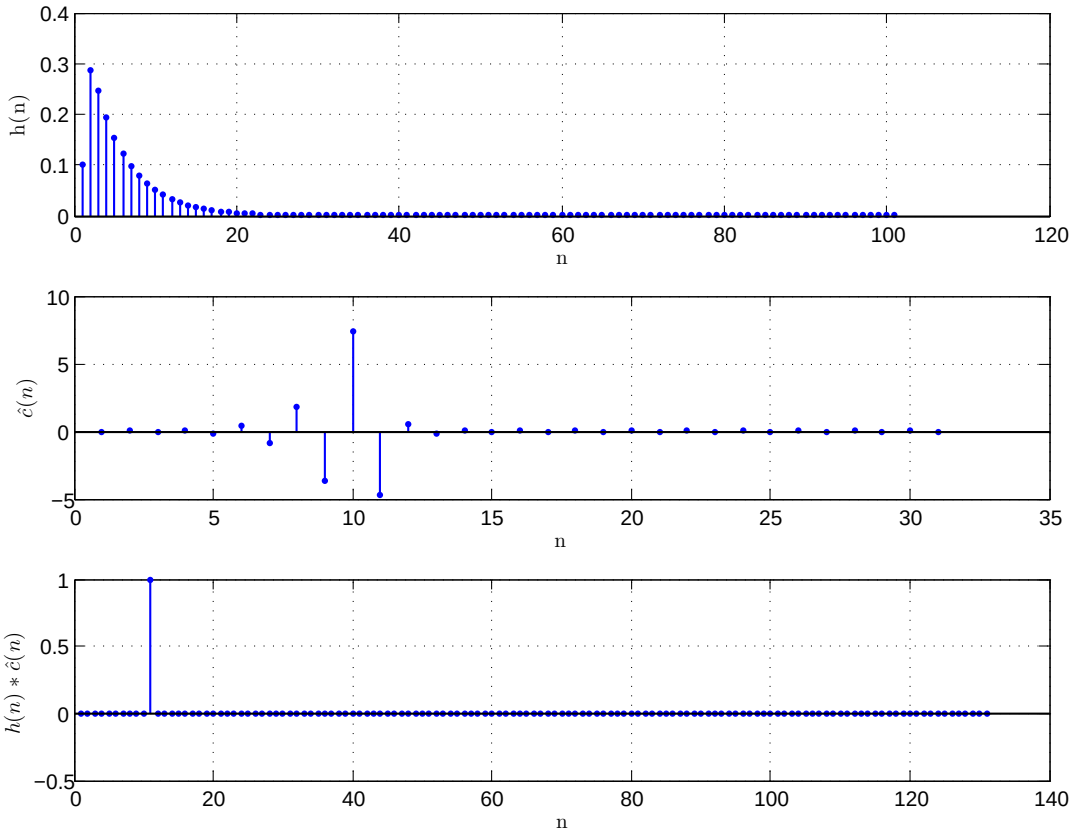

Figure 1.13: Results of convolution $h(n) * \hat{c}(n)$

we would not expect that the electrodynamic shaker system presents an unstable behavior.

1.3 Driving signals

Multiple transducers can be used to harvest electrical energy from the environment. Nevertheless, in most energy harvesting applications, electrodynamic and piezoelectric transducer are used to convert mechanical power in electrical power, since vibrations are present in every mechanical dynamic system. [1].

Some examples vibration sources [1]		
Vibration source	Peak acceleration $[\frac{m}{s^2}]$	Frequency $[Hz]$
Car engine compartment	12	200
Base of 3-axis machine tool	10	70
Car instrument panel	3	13
Person tapping his heel	3	1
Wooden deck with people walking	1.3	385
Window next to busy road	0.7	100
Washing machine	0.5	109
AC vents in office building	0.2-1.5	60
Refrigerator	0.1	240

There are three common techniques used in vibration testing: impulse (shock), sine sweep and random vibration. In general, the decision on which techniques to use depends on multiple factors. Moreover, every technique provides different characterization aspects of the device under test (DUT), such as resonance frequency, damping factors, mode shape and power profile in case of a piezoelectric generator.

1.3.1 Sine sweep testing

Sinusoidal or sine vibration testing is one of the more common and simple types of experiments performed in vibration test labs. Here the motion can be described by an oscillatory function such as the sine function. For a sinusoidal vibration, the relationship between acceleration, velocity and displacement is described by Eq. 1.13 and Eq. 1.14. Moreover, this relationship are frequency dependent and closely related through differential equations. [6].

$$v(t) = \frac{dx(t)}{dt} \tag{1.13}$$

$$a(t) = \frac{dv(t)}{dt} \tag{1.14}$$

where:
$a(t)$: is the acceleration $[\frac{m}{s^2}]$
$x(t)$: is the position $[m]$
$v(t)$: is the velocity $[\frac{m}{s}]$

In sine vibration testing, the following physical quantity are commonly used for the measurements of the vibration levels.

Acceleration: It is usually measured in its peak sinusoidal value and is expressed in $[\frac{m}{s^2}]$ or in normalized units of g, where the constant g is equal to the acceleration of gravity under standard conditions ($g = 9,81\ [\frac{m}{s^2}]$).

Velocity: It is specified in peak amplitude as well. It is expressed in $[\frac{m}{s}]$ and not often used in vibration testing.

Displacement: It is usually expressed in $[m]$ and measured in peak amplitude as well, or sometime over the total vibration excursion (peak to peak amplitude) [20].

As stated previously, these quantities are related to each other by the frequency of the sinusoidal vibration. According with this, the sinusoidal relations between acceleration, velocity and displacements are as follows.

$$A = 4\pi^2 f^2 D = 2\pi f V = \frac{V^2}{D} \tag{1.15}$$

were:

A : is the acceleration peak of $a(t)$ $[g]$
D : is the displacements peak of $x(t)$ $[m]$
V : is the velocity peak of $v(t)$ $[\frac{m}{s}]$
f : is the frequency $[Hz]$

Since the motion is sinusoidal also acceleration, velocity and displacement are sinusoidal. However, accordingly with the differential relationship expressed in Eq. 1.13 and Eq. 1.14, the phase between velocity and acceleration is 90° and the phase between displacement and acceleration is 180° (Figure. 1.14).

In a sinusoidal sweep, particular attention has to be reserved to the squared frequency relationship between displacement and acceleration (Eq. 1.15). For usual sine testing, the displacements above 100 Hz are generally small.
In contrast, for constant value of acceleration an decreasing value of frequency, the displacement increases rapidly. This can damage the vibration test system and the DUT.
As stated previously, in energy harvesting many tests use sine sweep vibration to

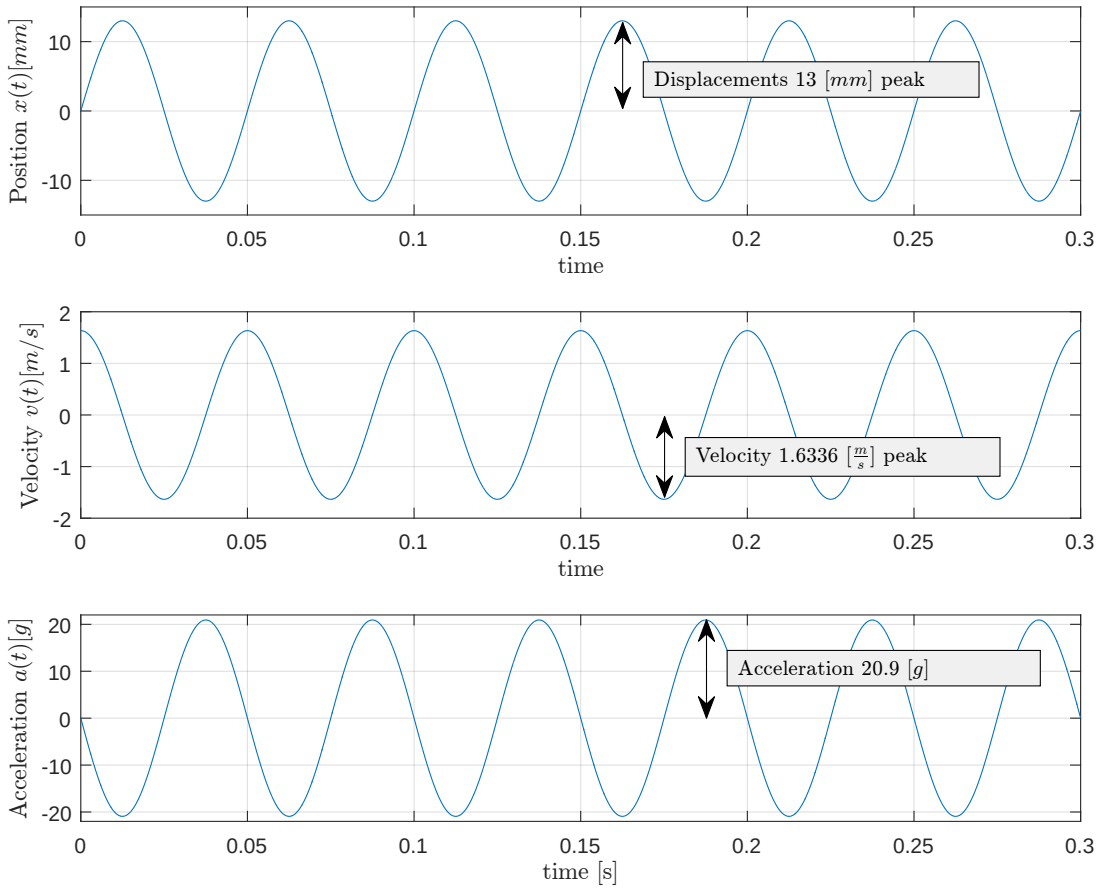

Figure 1.14: example of a $20Hz$ sinusoidal motion

identify resonances in piezoelectric generator, to characterize power performance in the frequency domain or for a modal analysis of the generator structure.
The sine sweep test can be achieved by starting at low frequency and sweep to the high frequency, or vice-versa. During the sweep, acceleration peak level A and the displacements D can be maintained constant or variable.
An accelerometer is used to provide the control feedback. It is fixed in the desired position of the load, and the acceleration profile is controlled during the whole vibration frequency sweep. Since the shaker has resonant frequencies, as explained in 1.2.1, if the resonant frequencies lie within the sweep band, the dynamic limits defined in the test equipment specification can be exceeded. This risk is usually prevented by using a closed loop control, it automatically adjust the driving signal to keep the acceleration peak value constant during the sweep.
Ideally the frequency range and time duration of a sine sweep has been predetermined an related to the expected frequency resolution of the test. The continuous

swept sine is achieved by varying the frequency of a sinusoidal function. Mathematically the function is defined as:

$$a(t) = A\sin(2\pi f(t)t + \varphi) \tag{1.16}$$

The amplitude A, and the phase φ are usually maintained constant during the sweep and the frequency $f(t)$ is a function of time. The test specification might require either a linear or a exponential sweep rate (Figure. 1.15). Exponential frequency increment (or decrement) spends greater time at the lower frequency with respect to a linear sweep. The relationship between frequency and time are expressed in (Eq. 1.17) (Eq. 1.18).

For a linear a sweep:

$$f(t) = f_{min} + (f_{max} - f_{min})\frac{t}{T_s} \tag{1.17}$$

for an exponential sweep:

$$f(t) = f_{min}\left[\frac{f_{max}}{f_{min}}\right]^{\frac{t}{T_s}} \tag{1.18}$$

where:
f_{max} : is the highest frequency in the sweep [Hz]
f_{min} : is the lower frequency in the sweep [Hz]
T_s : is the sweep duration [sec]
t : is the time [sec]

In this thesis, a linear sweep in the band $5 - 7000Hz$ is used to characterize the electrodynamic shaker and plot a frequency response as shown in Figure. 1.3 in 1.2.1.

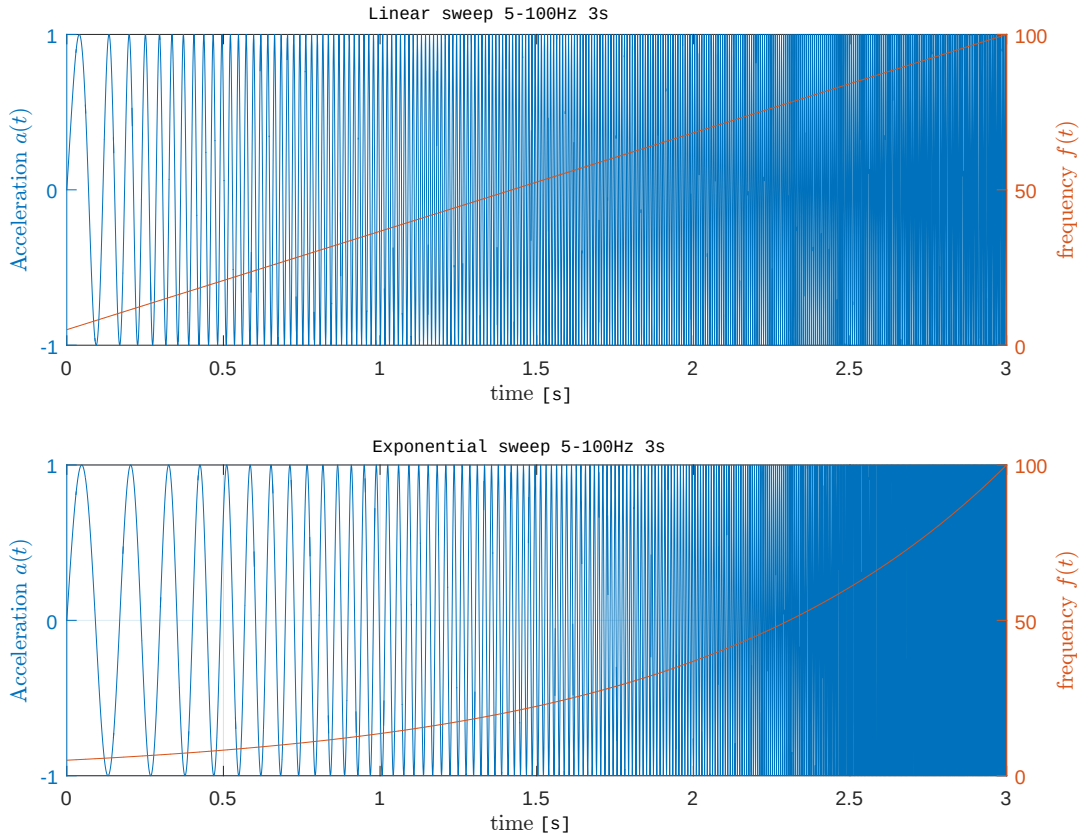

Figure 1.15: Sine sweep, linear and exponential

1.3.2 Environmental acceleration replication

Analysis of mechanical energy that can be harvested in real scenarios can be easily emulated in a laboratory, as an electrodynamic shaker can be used to reproduce pre-recorded acceleration data acquired in real environment.

In other words, time acceleration replication allows for reproducing long duration time waveforms in the lab instead of in the real environment. For example, by reproducing recorded data from road, cars, trains, aeroplanes etc. a more realistic vibration environment can be reproduced, assuring a higher level of certainty on the device performance.

Simulation of real vibration requires the integration of different processes and tools. The general procedure is illustrated in Figure. 1.16.

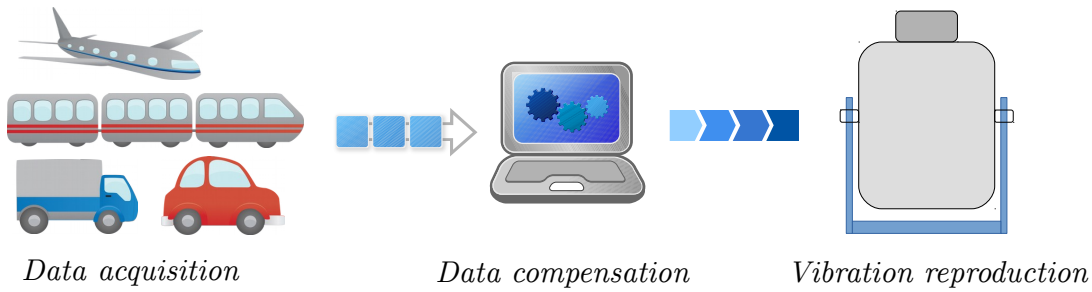

Figure 1.16: Process of data acquisition, compensation and reproduction by electrodynamic shaker

The acceleration data must be collected using a portable data logger, however on-field processing of data is usually problematic, and there is no guarantee whether the desired vibration signals have been captured until the data is returned to the testing lab. Before the data can be used for simulation, a compensation process is required. In a data compensation process, the signal is conformed to the physical limit of the shaker, potential DC offset are removed, and eventually up-sampling conversions are carried out.

The first factor to consider is the dynamic range of the shaker, in term of displacement, maximum force and maximum velocity, to be certain the acceleration profile can be applied to the shaker. However, in energy harvesting the mechanical energy is usually limited, and this is not a big obstacle. The second factor to analyse is the power spectral density of the vibration signal. A recorded signal can contain significant components at low frequencies, due to slow variation of the vehicle position. Such components are typically below $5Hz$ and can represent a problem because of the displacement limitation. Furthermore, these low frequency

components are not of interest in typical energy harvesting applications, and can be removed without a significant change in power analysis.

Figure. 1.17 shows the Matlab user interface used in this thesis to analyse and compensate the long time recorded data, offline on a PC. This software provides the compensation necessary to prepare a signal for laboratory replication.

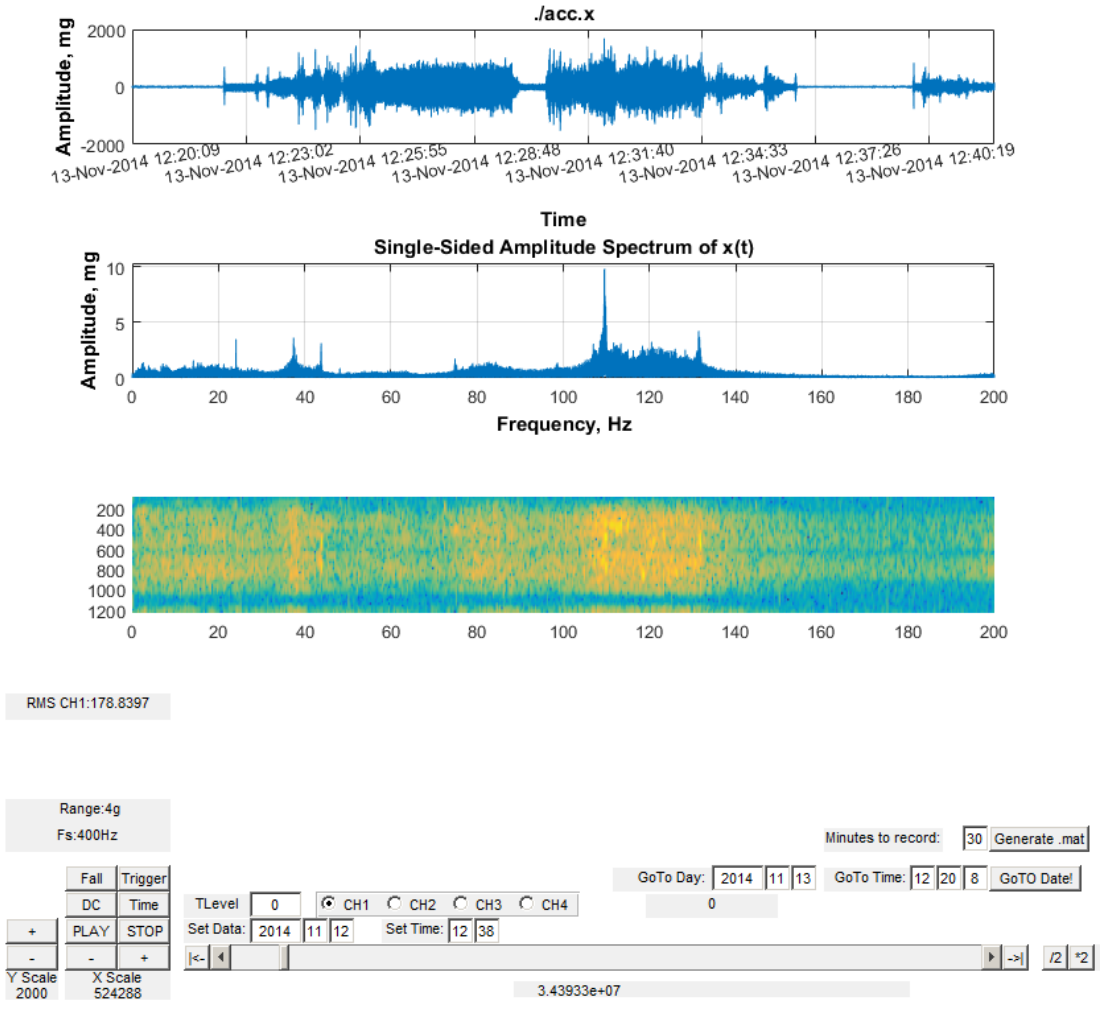

Figure 1.17: Matlab interface used for data splitting, analysis and compensation.

Figure. 1.18 shows the results of a realistic data compensation process for an acceleration signal recorded on a plane with a sampling frequency $Fs = 400Hz$. The first step is to apply an high-pass filter in order to remove the low frequency components below $5Hz$. The second step is an up-sampling conversion with the

aim to match the sampling frequency of the digital to analog converter (DAC). Finally the compensated signal can be used for vibration replication.

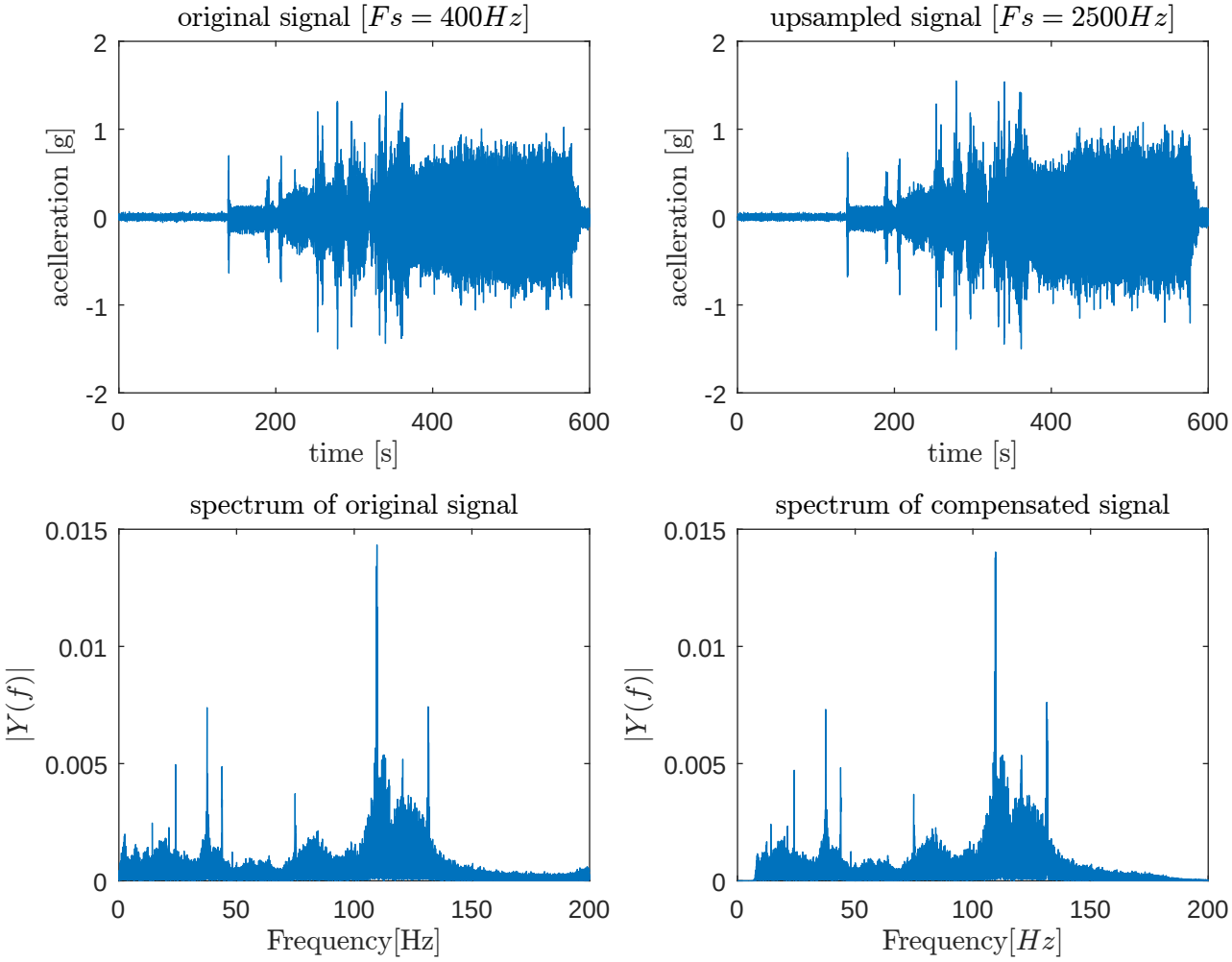

Figure 1.18: Real signal, before and after compensation in the band $[5 - 200]Hz$

During the test, the signal is streamed from the hard drive to the shaker control software, which uses a closed loop to monitor the response of the shaker as the test is conducted. The control loop developed in this thesis uses an adaptive algorithm which continuously computes the drive signal based on the system transfer characteristic. In this way the control accuracy is higher than an open-loop solution [21]. Furthermore, the driving signal is computed in real-time, based on the current system transfer characteristic and the control loop can respond to a system change.

The shaker control software interface (Figure. 1.19) provides the status of the

test. The current waveform form, the RMS value of the error (calculated as distance between desired and actual acceleration signal) and the FIR filter coefficients are shown.

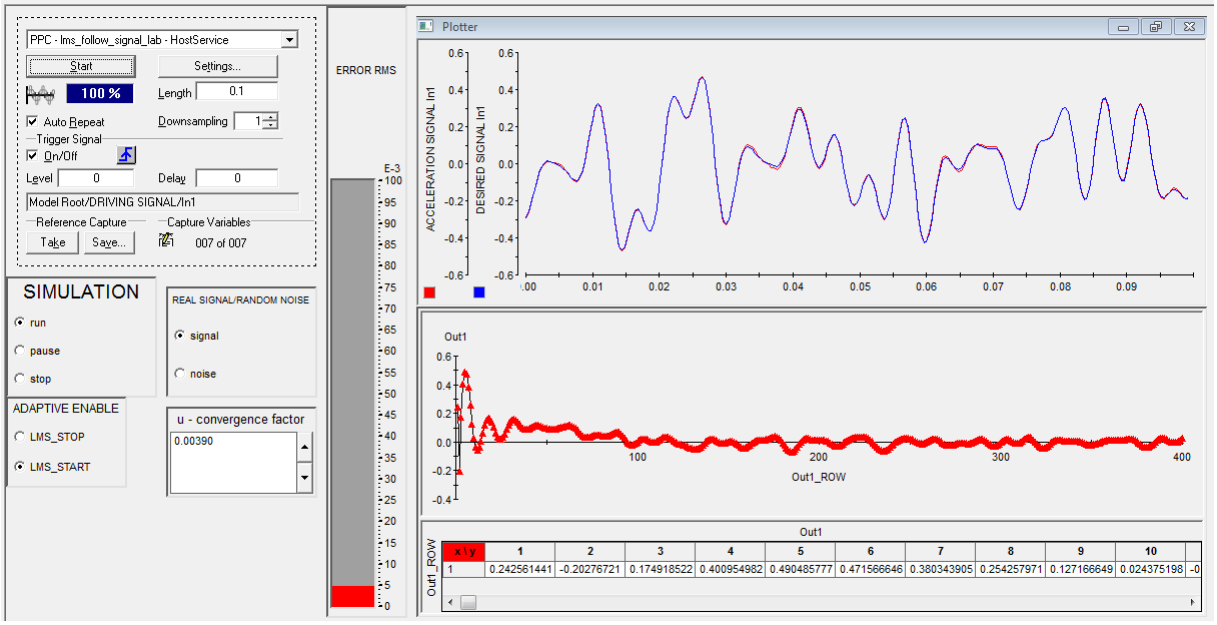

Figure 1.19: Shaker control interface during a real signal simulation in the band $5 - 200Hz$

This page intentionally left blank.

Chapter 2

Overview of acceleration control system

2.1 Introduction

In this chapter, the vibration control loop shown in Figure. 2.1 is analysed, particular attention is dedicated to the electrodynamic shaker characterization. In fact, it plays a fundamental role in the experimental set-up and its transfer function defines the relationship between the mechanical and electrical domain.
Several undesired effects that make a control loop useful are discussed. The most important aspect to consider is the complex relationship between the electric signal at the power amplifier input and the electrical signal provided by the accelerometer mounted in the location of interest. In general this relationship is frequency and time dependent. However, the time dependency due to factors such as temperature or the aging of the components is generally slow if compared to the dynamics of the system. Slow variations in the characteristics are not analysed in this thesis, and a compensation for this factor is demanded from the adaptive real-time control.
The power amplifier presents an almost flat transfer function when it is used in voltage mode, and the voltage applied to the shaker can be considered a proportional copy of the input signal.
In this chapter, the transfer function of the electrodynamic shaker is defined by experimental measurements and a two degree of freedom (2DOF) model presented in [21]. Mechanical characteristics, like resonance, damping and rotational moments, make the transfer function not only frequency dependent but also dependent from the accelerometer position.
These set of dependencies make the use of an adaptive closed loop solution highly recommended. Most systems use acceleration for their control feedback [22]. A feedback signal is produced by using a lightweight accelerometer with appropriate

characteristics in term of bandwidth, range and sensitivity [23].
The accelerometer can be positioned on the shaker test table, on the specimen, or in other critical positions. Furthermore, multiple accelerometers can be used to monitoring complex structure [24].

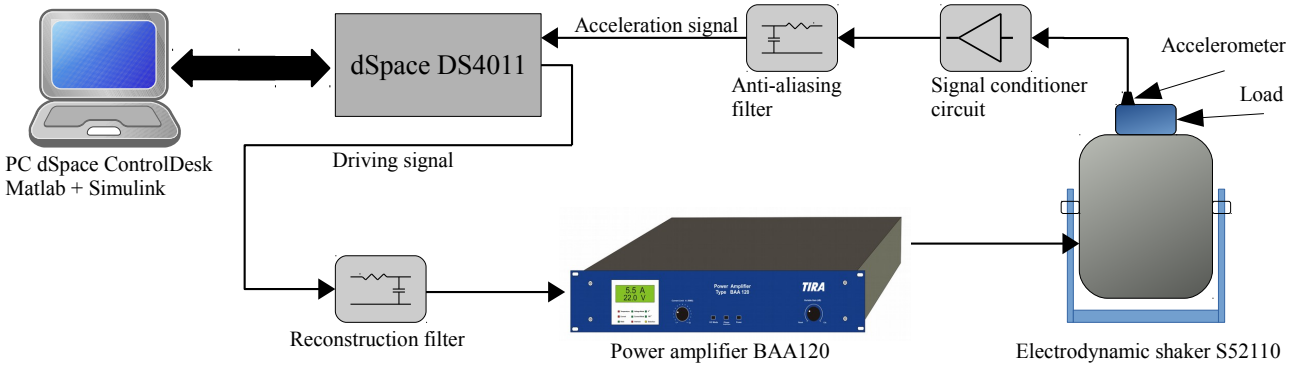

Figure 2.1: Vibration control system set-up used in this tesis

2.2 Electrodynamic Shaker

The electrodynamic shaker used in this thesis is the model S52110 from TIRA. (Figure. 1.1b) [5]. The specification is given in Figure. 2.2.

Different techniques, with different levels of representation, are proposed in

TECHNICAL PARAMETERS Vibration exciter S 52110

Rated peak force $Sine_{pk}$/$Random_{RMS}$	100/50 N
Frequency range	2-7000 Hz
Main resonance frequency	>5700 Hz
Max. displacement Peak-Peak	15 mm
Max. velocity Sine/Random	1.5/1.5 m/s
Max. acceleration Sine/Random	50/25 g
Suspension stiffness	5 N/mm
Effective moving mass	0.25 kg
Weight	36 kg
Armature diameter	60 mm

Figure 2.2: Electrodynamic shaker specifications

literature to model an electrodynamic shaker [4, 6, 21, 25]. In this chapter, a

two degree of freedom (2DOF) model is used for the mechanical part, and an experimental test is set-up in order to compute the frequency response of the shaker. The 2DOF model is then completed by known and estimated parameters with the aim to match the experimental transfer function.

2.2.1 Electrical model

As described in chapter 1.2.1, the electrodynamic shaker is composed basically of a moving coil suspended in a radial magnetic field and fixed to a moving element called armature. When the coil undergoes a current i_a, an axial force f_{em} is produced and transmitted to the moving elements. With the aim to simplify the model, the magnetic flux density in the magnetic field is considered constant, so the generated force can be expressed as $f_{em} = \Gamma i_a$ (Eq. 1.1). In the electrical domain, the shaker model can be represented by a resistance R in series with an inductance L and a voltage generator (Figure. 2.3). The voltage generator e, represents the back electromotive force, which is generated across the coil when it moves in the magnetic field (Eq. 1.3). Therefore, current and voltage at the coil are related to each other by differential equations (Eq. 1.2).

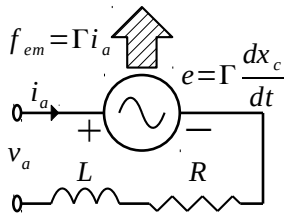

Figure 2.3: Moving coil electrical model.

The coil resistance R and inductance L were measured off-line through an LCR meter while blocking the armature in order to set the back EMF to zero. In general R and L have a non linear frequency dependency, because of the skin effect and the action of pole plating in the shaker, which increase the resistance and decrease the inductance with frequency [6, 21]. However, in order to simplify the model, resistance and inductance were assumed constant end equal to the measured value at $2KHz$ ($R = 4\Omega$, $L = 138\mu H$).

2.2.2 Mechanical model

In order to define a simplified (but representative) mechanical model of the shaker, some assumptions are considered. First, the shaker structure is assumed rigidly fixed to the building floor, and used as reference. Second, the test load is assumed free of resonance and rigidly attached to the moving elements of the shaker. Under

these assumption, the mechanical model can be represented as a two degree of freedom 2DOF system as shown in Figure. 2.4.

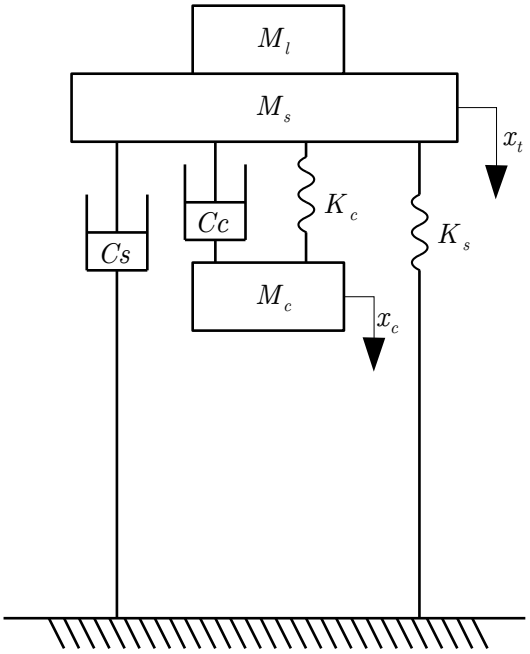

Figure 2.4: Mechanical model.

Where:
M_l : is the load mass [kg]
M_s : is the table mass [kg]
M_c : is the coil mass [kg]
K_c : is the stiffness of the adhesive bonding used to fix the coil $[\frac{N}{m}]$
K_s : is the stiffness of the shaker suspension $[\frac{N}{m}]$
C_c : is the damping coefficient of the adhesive bounding used to fix the coil $[\frac{N \cdot sec}{m}]$
C_s : is the damping coefficient of the shaker suspension $[\frac{N \cdot sec}{m}]$
x_t : is the table displacement to the floor $[m]$
x_c : is the coil displacement to the floor $[m]$

Considering Hooke's law for a linear spring, the reaction force produced by a compressed spring can be written as Eq. 2.1:

$$f_{sp} = -Kx \tag{2.1}$$

Where:

K_c : is the spring stiffness $[\frac{N}{m}]$
x : is the displacement

Moreover, the friction force of the damper is proportional to the velocity, and can be written as Eq. 2.2:

$$f_d = -C\frac{dx(t)}{dt} \tag{2.2}$$

Where:
C : is the damping coefficient $[\frac{N \cdot sec}{m}]$
x : is the displacement

Therefore, Newton's second law of motion permits to write two equations as the sum of applied force in the axial direction to the coil mass (Eq. 2.3(Eq. 2.4):

$$f_{em} = \Gamma i_a = M_c\frac{d^2x_c(t)}{dt^2} + C_c(\frac{dx_c(t)}{dt} - \frac{dx_t(t)}{dt}) + K_c(x_c - x_t) \tag{2.3}$$

and

$$C_c(\frac{dx_c(t)}{dt} - \frac{dx_t(t)}{dt}) + K_c(x_c - x_t) = (M_l + M_s)\frac{d^2x_t(t)}{dt^2} + C_s\frac{dx_t(t)}{dt} + K_s x_t \tag{2.4}$$

Combining the two equation above, use a Laplace transform, a transfer function can be written as:

$$H_{ia}(s) = \frac{a(s)}{i(s)} \tag{2.5}$$
$$= \frac{x_t(s)s^2}{i_a(s)}$$
$$= \frac{\Gamma(C_c s + K_c)s^2}{M_c(M_l + M_s)s^4 + (M_c C_s + C_c M)s^3 + (M_c K_s + C_c C_s + K_c M)s^2 + (C_c K_s + K_c C_s)s + K_c K_s}$$

where: $M = M_c + M_s + M_l$.

Some considerations can be made on the the transfer function H_{ia} with the aim to identify the mechanical parameters. As stated in chapter 1.2.1, in the low end of the operative range, the armature and the coil move together, relative to the shaker body. Therefore coil mass, table mass and load mass can be considered a rigid body with a single mass, that combined with suspension spring and damper define the shaker suspension mode. In this low frequency range, the damping coefficient C_c and stiffness K_c can be considered both infinite, and the transfer function can be simplified as below (Eq. 2.6).

$$H_{iaL}(s) = \frac{\Gamma s^2}{(M_c + M_l + M_s)s^2 + C_s s + K_s} \tag{2.6}$$

When the shaker has no load ($M_l = 0$), the suspension resonance frequency can be calculated as Eq. 2.7:

$$f_{0L} = \frac{1}{2\pi}\sqrt{\frac{K_s}{M_s + M_c}} \tag{2.7}$$

that can be experimentally identified based on the $+90°$ phase shift. Now a known inertial load can be applied on the table test ($M_l \neq 0$), therefore the resonant frequency is reduced to Eq. 2.8.

$$f_{lL} = \frac{1}{2\pi}\sqrt{\frac{K_s}{M_s + M_c + M_l}} \tag{2.8}$$

Like in the no-load condition, the resonance frequency can be identified experimentally based on the $+90°$ phase shift. Then, based on the measured resonance frequencies, the moving mass of the shaker and the suspension stiffness can be estimated.

$$M_o = (M_c + M_s) = \frac{f_{lL}^2}{f_{0L}^2 - f_{lL}^2} M_l \tag{2.9}$$

$$K_s = (2\pi f)^2 M_o \tag{2.10}$$

The same considerations can be made at high frequencies. In this frequency range, the coil mass and the table mass move out-of-phase because of the adhesive bonding, so that C_s and K_s can be set equal to zero and the transfer function can be approximated to Eq. 2.11.

$$H_{iaH}(s) = \frac{\Gamma K_c}{M_c(M_l + M_s)s^2 + (M_l + M_o)C_c s + (M_l + M_o)K_c} \tag{2.11}$$

In no-load condition ($M_l = 0$), the resonance frequency is Eq. 2.12,

$$f_{0H} = \frac{1}{2\pi}\sqrt{\frac{M_o K_c}{M_s M_c}} \tag{2.12}$$

as well, in a known-load condition the resonance frequency is Eq. 2.13.

$$f_{lH} = \frac{1}{2\pi}\sqrt{\frac{(M_l + M_o)K_c}{(M_l + M_s)M_c}} \tag{2.13}$$

Therefore, based on the experimental measurements of the high resonant frequencies, the coil mass M_c, the table mass M_t and the coil stiffness K_c can be estimated (Eq. 2.14) (Eq. 2.15) (Eq. 2.16).

$$M_c = \frac{(f_{0H}^2 - f_{lH}^2)(M_l + M_o)M_o}{f_{0H}^2(M_l + M_o) - f_{lH}^2 M_o} \tag{2.14}$$

$$M_t = M_o - M_c \tag{2.15}$$

$$K_c = \frac{M_s M_c}{M_o}(2\pi f_{0H})^2 \tag{2.16}$$

The remaining parameter C_s , C_c, and Γ can be evaluated by experimental observation as follows.
The shaker ratio of thrust to coil current Γ (Eq. 1.1) can be evaluated in no load condition (Eq. 2.17) by considering the module of (Eq. 2.6), far away from the low resonance frequency (usually $f \geq 10 f_{0L}$), in the constant acceleration region (Figure. 1.2).

$$\Gamma = M_o \Big| H_{iaL}(j2\pi 10 f_{0L}) \Big|_{M_l=0} \tag{2.17}$$

Furthermore, the damping coefficient of the shaker suspension C_s can be estimated by considering the module of Eq. 2.6 at the resonance frequency, in no load condition (Eq. 2.18).

$$C_s = \frac{2\pi f_{0L}\Gamma}{\Big| H_{iaL}(j2\pi f_{0L}) \Big|_{M_l=0}} \tag{2.18}$$

Lastly, the damping coefficient of the coil adhesive bonding C_c, can be estimated considering the module of (Eq. 2.11) at the hight resonance frequency, in no load condition (Eq. 2.19).

$$C_c = \frac{K_c\Gamma}{2\pi f_{0H} M_o \Big| H_{iaH}(j2\pi f_{0H}) \Big|_{M_l=0}} \tag{2.19}$$

2.2.3 Transfer function of the electrodynamic shaker

The electrical and mechanical model can now be connected to complete the electromechanical model (Figure. 2.5).

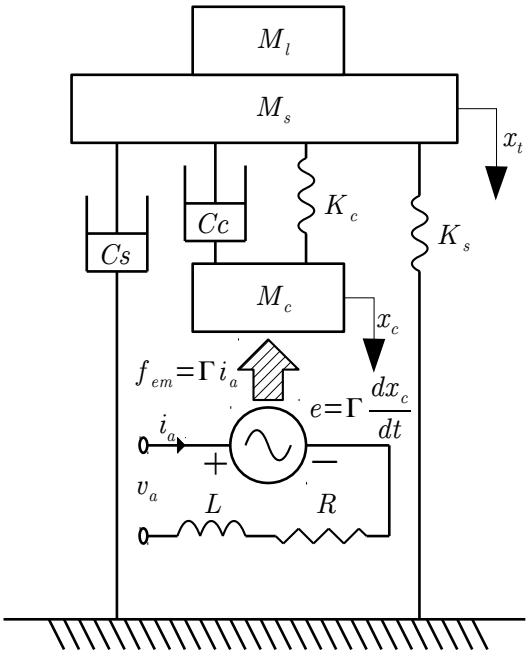

Figure 2.5: Shaker electromechanical model.

For the experimental validation of the model, the electrodynamic shaker type $S52110$ driven by power amplifier $BAA120$ (both manufactured dy TIRA) was used (Figure. 2.6). The frequency response of the shaker is carried out by feeding the shaker with a constant amplitude sinusoidal sweep signal provided by a function generator. During the sweep, the shaker voltage, current and the armature acceleration was recorded on a PC by a dSPACE DS1104 controller board.
The signal, swept from $9Hz$ to $7kHz$, is generated from the Agilent 33250A function generator. Moreover, the frequency was increased exponentially in order to have a good analysis also in the low frequency range. The acceleration output response was measured by an accelerometer model $M352C68$ manufactured by PCB, and the frequency response was computed as the ratio between the output acceleration and the signal acquired from the current monitor port in the back of the power amplifier.

The suspension mode resonance frequency at $38.15Hz$, and the coil mode resonance frequency at $6058.20Hz$ can be extracted from the measured frequency response of the unloaded shaker (Figure. 2.8). For load conditions, a $0.427kg$ of

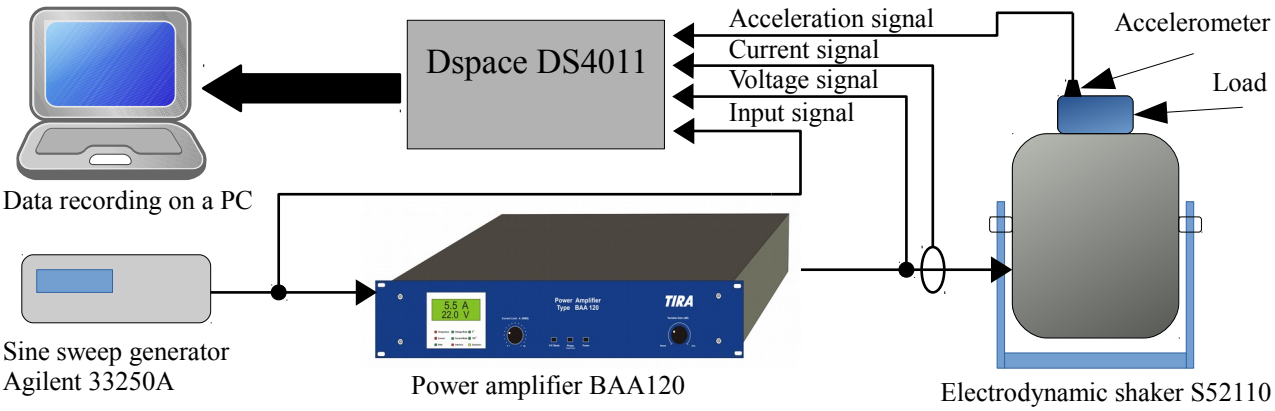

Figure 2.6: Laboratory set-up for frequency response measurement.

aluminium mass was used as test load to characterize the Shaker (Figure. 2.7b). For the loaded shaker (Figure. 2.9), the suspension mode resonance frequency is measured at $26.17Hz$ and the coil mode resonance frequency at $5155.20Hz$.

The resulting identified mechanical parameters are shown below.

Electrodynamic shaker identified mechanical parameter		
Parameter	Symbol	Value
Coil mass	M_c	$0.1588[kg]$
Coil bounding stiffness	K_c	$133.381 \cdot 10^6[\frac{N}{m}]$
Coil dumping coefficient	C_c	$60.6200[\frac{N \cdot sec}{m}]$
Table mass	M_s	$0.2207[kg]$
Suspension stiffness	K_s	$17557[\frac{N}{m}]$
Suspension dumping coefficient	C_s	$4.3260[\frac{N \cdot sec}{m}]$
Force generation constant	Γ	$2.5510[\frac{N}{A}]$

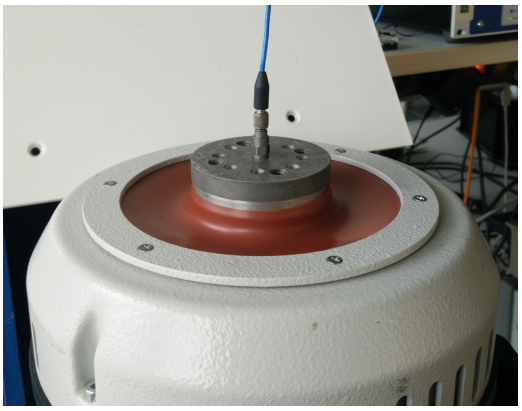

(a) Unloaded shaker

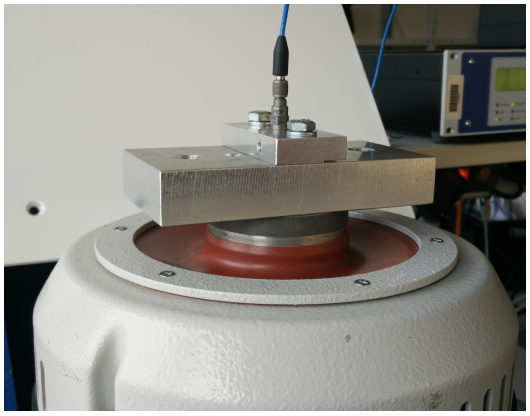

(b) $0.427Kg$ of aluminium mass

Figure 2.7: Loaded and unloaded electrodynamic shaker used for the transfer function estimation

In conclusion the simulated response obtained from the two degree of freedom model is a good approximation of the shaker dynamic behaviour (except for some small resonances), in the useful frequency range. Above the coil resonance mode, the model loses accuracy.

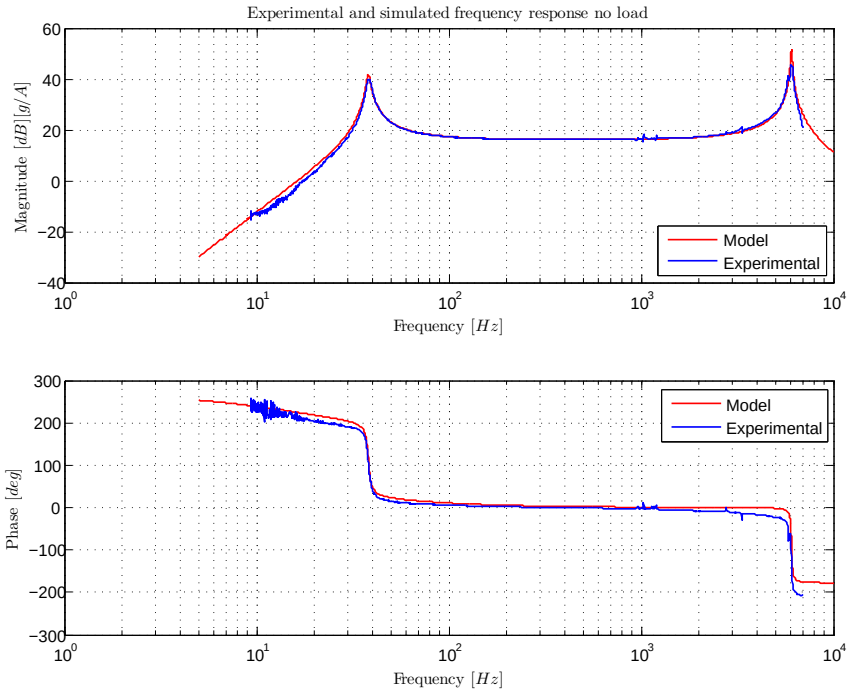

Figure 2.8: Experimental and simulated frequency response of $H_{ia}(s)$ without load.

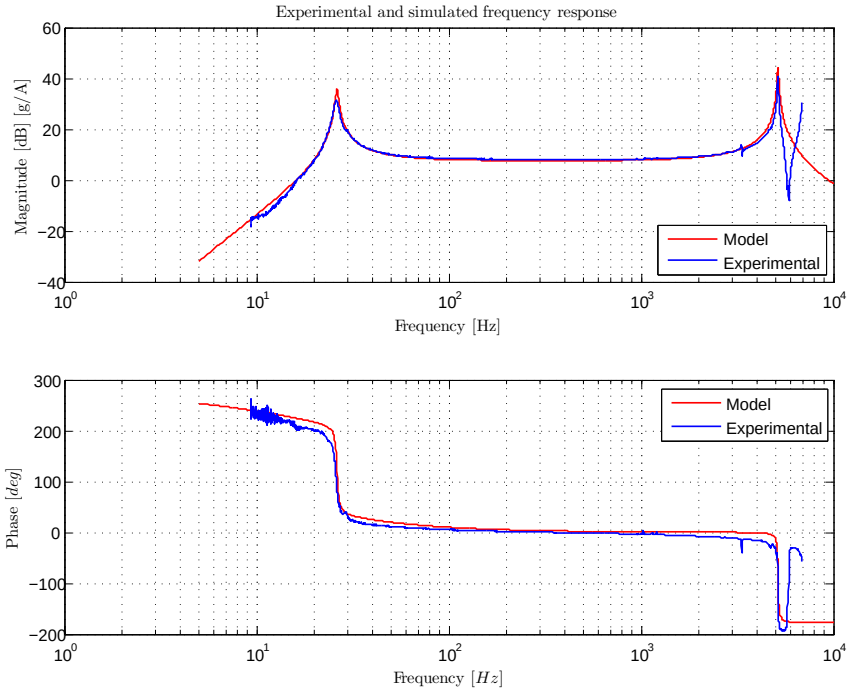

Figure 2.9: Experimental and simulated frequency response of $H_{ia}(s)$ with load.

2.3 Power amplifier

The power amplifier is used for signal amplification, in order to provide the necessary energy to the input signal before applying it to the electrodynamic shaker. The power amplifier used for vibration testing usually has a high quality, and is designed to satisfy selective requirements on distortion, noise, output current and reliability. The power amplifier must also have a capability to tolerate highly reactive loads, protection from short circuit, and over temperature condition. Usually the power stage employs an output current limiter, which limits the instantaneous positive and negative peaks of the output current. The output signal can be phase inverted ($0°or180°$), usually by a dedicated switch at the front panel. The power amplifier used in this thesis is of type BAA120 manufactured by TIRA (Figure. 2.10), and has the specification shown in Figure. 2.11.

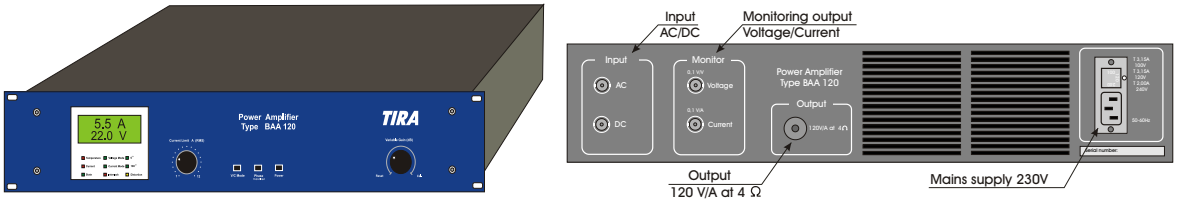

(a) Power amplifier front panel

(b) Power amplifier back panel

Figure 2.10: Front and back panel of the power amplifier [5]

TECHNICAL PARAMETERS Power Amplifier BAA 120

Output power$_{RMS}$	120 VA
Frequency range	DC - 20 kHz
Voltage-/Current mode	yes/yes
Voltage$_{RMS}$, max.	22 V
Current$_{RMS}$, max.	5.5 A
Load resistance, opt.	4 Ohm
Signal input voltage$_{RMS}$	< 5 V
Distortion	< 0.1 %
Signal to noise ratio	> 90 dB
Weight	16 kg
Dimensions (WxHxD)	483 x 90 x 450 mm
Power supply (Standard)	1~ / N / PE 230 V±5% 50 Hz CEE 7/7
Recommended fuse protection (Standard)	16 A slow
Max. power consumption at 230 V	0.08 kVA
Interlocks:	Overload, Temperature, Clipping

Features:
High Signal to noise ratio of >90 dB

Figure 2.11: Power amplifier BAA120 specifications

2.3.1 Transfer function of the power amplifier

In order to measure the transfer function of the power amplifier, the same set-up as shown in Figure. 2.6 was used. The frequency response measurement of the power amplifier is carried out by feeding the amplifier with a constant amplitude sinusoidal sweep signal provided by a function generator. During the sweep test, the input and output signal was recorded on a PC by a dSPACE DS1104 controller board. The measured transfer function is shown in Figure. 2.12.

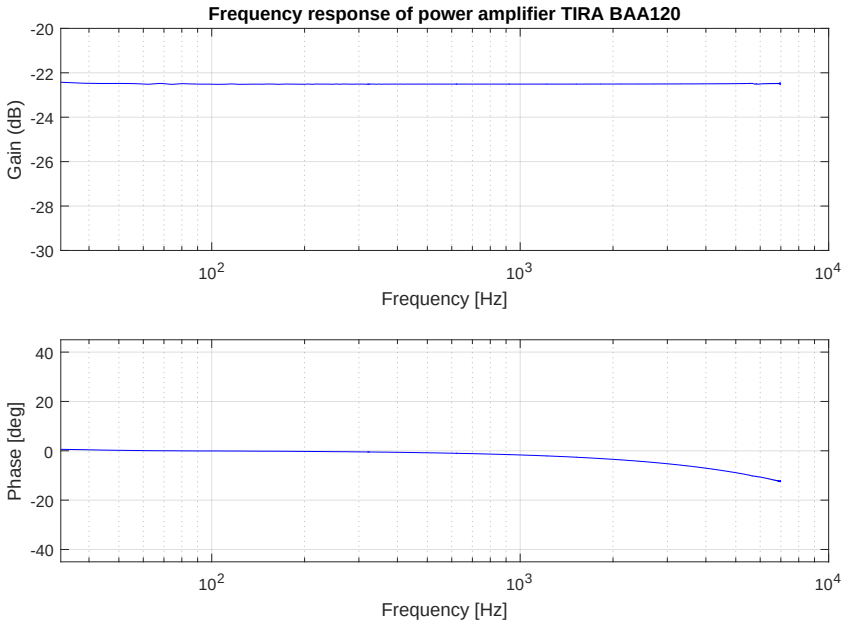

Figure 2.12: Experimental frequency response of power amplifier BAA120.

In Figure. 2.12 it is possible to observe the flat response of the power amplifier, at least in the useful frequency range. Due to the fact that the frequency response has an almost constant phase and gain in the frequency range, the transfer function for the power amplifier can be approximated as a constant multiplicative gain K_a, depending from the the gain control knob at the power amplifier front panel (Eq. 2.20).

$$H_{pa} = K_a \tag{2.20}$$

2.4 Accelerometer and signal conditioning

To measure and characterize vibration, accelerometers are the most employed sensors. The main advances of this sensor are the absolute acceleration measurement (no external reference point is needed) and the possibility to apply it directly on the vibration structure.
The piezoelectric accelerometers are relatively lightweight, and the mass of the accelerometer is usually negligible respect to the whole moving mass [1].
Piezoelectric accelerometers are mostly used for measuring vibration, and are usually fixed to a moving part in order to sensing the acceleration in the mounting position.
Piezoelectric accelerometers have also wide dynamic range, good linearity and are relatively durable. A piezoelectric transducer is an electromechanical device that generates an electric signal when subjected to a variable force.
This is accomplished with a seismic mass m which experiences a dynamic force F when they are accelerated, according to the Newton's Second Law of Motion $F = ma$.
This force is then applied to a crystal element that converts it in to a voltage. The basic design of an accelerometer can be represented as a one degree of freedom 1DOF system shown in Figure. 2.13a.

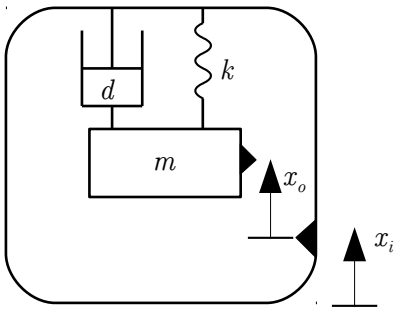

(a) Basic accelerometer block diagram

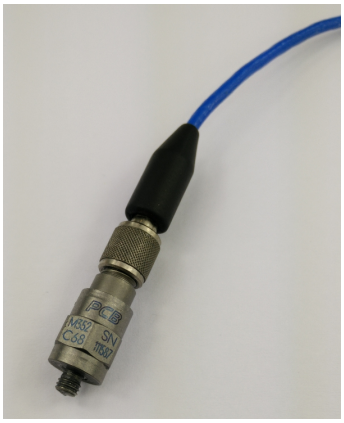

(b) Piezoelectric accelerometer used in this thesis

Figure 2.13: Piezoelectric accelerometer

An elastic suspension with stiffness k and damping d connect the moving mass to the frame of the sensor. The frame of the sensor is fixed on the vibrating structure and moves integral with it.
Therefore, this system is defined by the following differential equation (Eq. 2.21).

$$\frac{d^2x_o}{dt} + 2\xi\omega_0\frac{dx_o}{dt} + \omega_0^2 x_o = -\frac{d^2x_i}{dt} \tag{2.21}$$

with ω_0 as resonance frequency and ξ is the damping ratio:

$$\omega_0 = 2\pi f_0 = \sqrt{\frac{k}{m}} \tag{2.22}$$

$$\xi = \frac{d}{2\omega_0 m} \tag{2.23}$$

From the differential equation some considerations can be derived. With the aim to measure acceleration, the displacement x_0 must be proportional to the acceleration $\frac{d^2x_i}{dt}$. This is true if the term $\omega_0^2 x_o$ is dominant in Eq. 2.21, and if its true, the differential equation can be simplified as Eq. 2.24.

$$\omega_0^2 x_o = -\frac{d^2x_i}{dt} \tag{2.24}$$

Piezoelectric accelerometer usually have a very high resonance frequency ($10 \ldots 100kHz$), that allow to use it in a wide frequency range. Figure. 2.14 show the frequency response of the piezoelectric accelerometer used in this thesis.

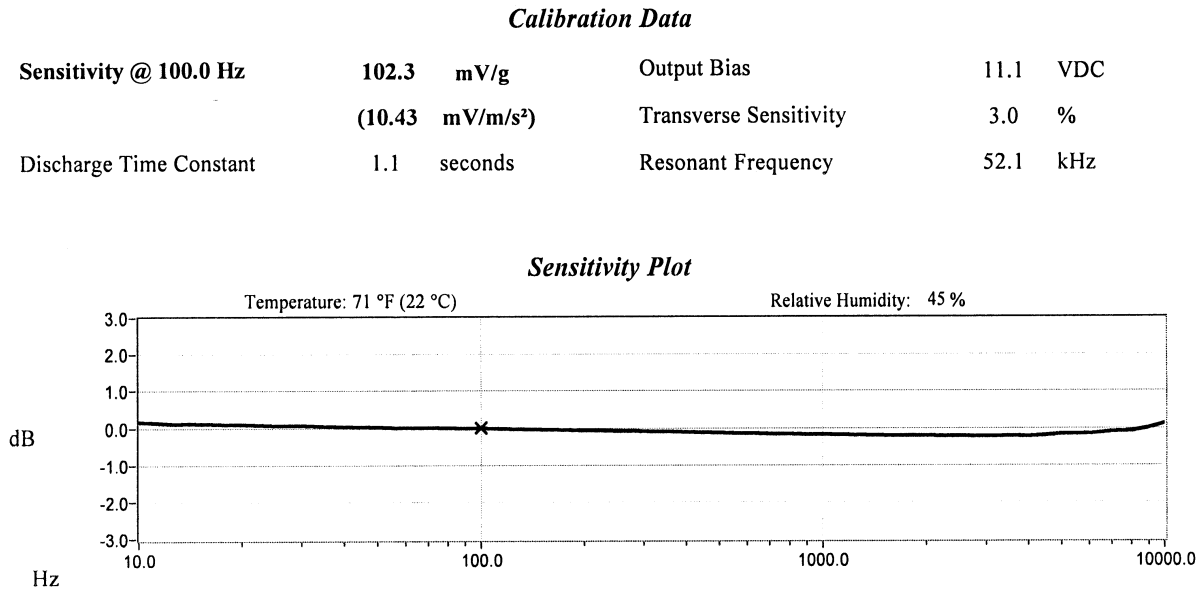

Figure 2.14: Frequency response of the accelerometer $PCB - M352C68$ used in this thesis [26].

A piezoelectric accelerometer sensor usually requires a constant current source. The signal conditioner consists of a well-regulated 18 to 30 VDC source (line-powered LDO), a constant current generator, a decoupling stage used to remove the DC component of the signal and an amplification stage. (Figure. 2.15).

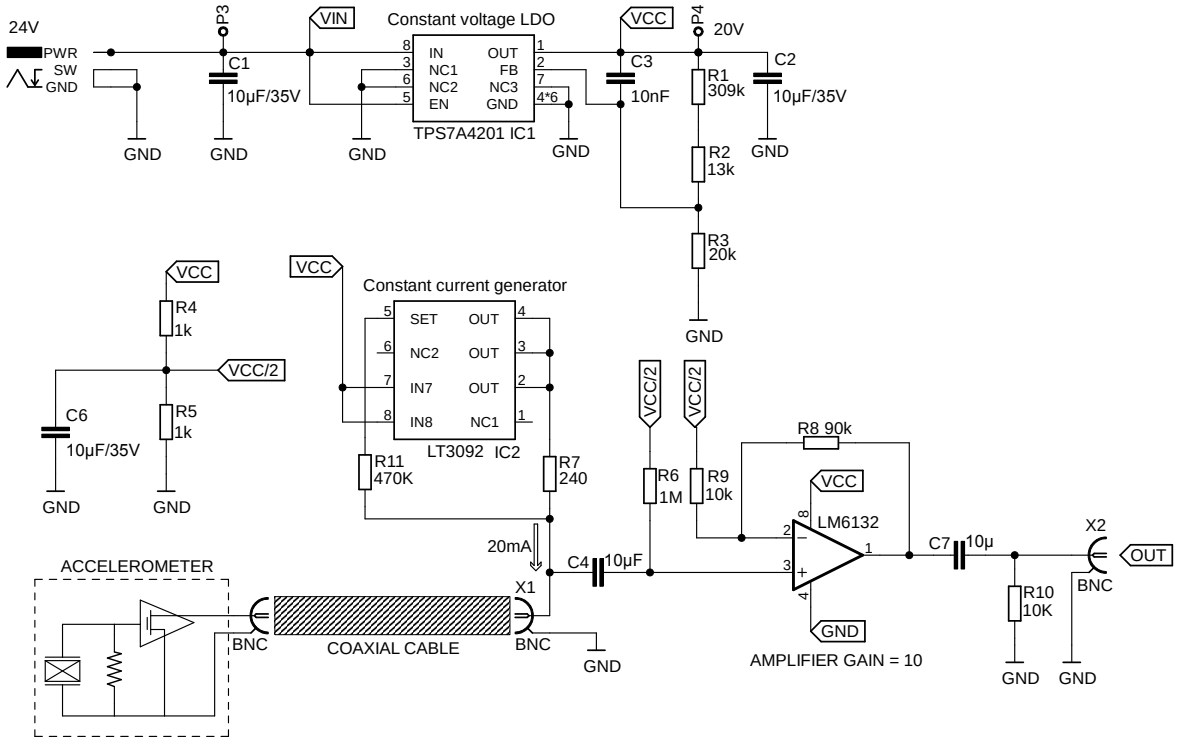

Figure 2.15: Acceleration signal conditioner circuit.

The constant current generator is required by the accelerometer, moreover, it can be modified to supply higher currents for driving long cable lengths (high parasitic capacitance). The acceleration signal is then decoupled by the $10\mu F$ capacitor in order to eliminate the sensor bias voltage.

Finally, an operational amplifier is used to increase the output signal level. In energy harvesting applications, typical levels of ambient vibrations are around $0.1g$. Therefore, the sensor output voltage is very limited to employ the full resolution of the ADC converter, so an external amplifier is used to ensure that the maximum amplitude range of the signal to be measured is mapped to the full scale range of the ADC, (which is ± 10V). For a readout device having a very high input impedance (as encountered with some operational amplifier or ADC converter), it may be necessary to place a 10 Kohm resistor in parallel to the read out input to eliminate the slow turn-on and signal drift. This provides a zero-based, AC-coupled output signal that is compatible with most standard readout device. After completing the

system set-up and switching on the signal conditioner, 1 to 2 minutes are needed for the system to stabilize.

2.5 Anti-aliasing and reconstruction filters

The anti-aliasing filter on the signal conditioner output (Figure. 2.1) is used to remove every spectral components above half the sampling frequency, accordingly whit the Niquist sampling theorem.

ensure that any frequency components above half the sampling frequency are removed, otherwise they are aliased to lower frequencies. The reconstruction filter at the digital to analog converter output, is necessary for removing the reflected spectrum of the analog signal produced by the digital to analog conversion at frequency above half the sampling frequency. The anti-aliasing filter and reconstruction filters are both first order low-pass R-C filter. The reason for choosing a simple R-C filter for anti aliasing protection is the limited band of the signal ($f_{max} = 200Hz$) compared to the sampling frequency ($5kHz$). However, if the band of the signal increases, it might not be enough, and a high-order filter with great attenuation (elliptic filter as an example) has to be used [27].

2.6 Controller Board - DS1104

In this thesis the controller Board DS1104 from dSPACE GmbH based on a Power PC was used to implement and test the real-time control algorithm. The DS1104 Controller Board is a PCI card based on 64-bit floating-point processor MPC8240, PowerPC 603e, running at 250 MHz (Figure. 2.16a). For purposes of fast prototyping, the CP1104 Connector Panel provides rapid connections with the DS1104 (Figure. 2.16b).

(a) dSPACE DS1104 R&D Controller Board (b) Connector panel CP1104

Figure 2.16: dSPACE DS1104 R&D Controller Board and connector panel CP1104

The DS1104 PCI Card is installed on the motherboard of the laboratory computer, and connected to the CP1104 Connector Panel via a master I/O ribbon cable. The board include also a slave DSP TMS320F204 for advance digital I/O control. (complete list of characteristics can be found in the DS1104 manual).
The DS1104 real-time hardware is controlled by the Platform Manager integrated in the software ControlDesk, that permits to control variables, plot signals, record signals and replay pre-recorded signals (Figure. 1.19) [28].
Implementing a control algorithm can either be done by embedding the blocks provided by dSPACE's Real-Time Interface (RTI) in a Simulink model or using real time library functions to handcode the application directly in C. Then, the control algorithm is built and download to the dSPACE real-time hardware. While the application is running on the dSPACE board, the ControlDesk software is used for the signal observation and for changing the parameters of the real-time application. The real-time control of a continuous system by a discrete controller is triggered by the sampling time period of T. Figure. 2.17 show the connections between the physical system and the controller implemented on the dSPACE board [29].

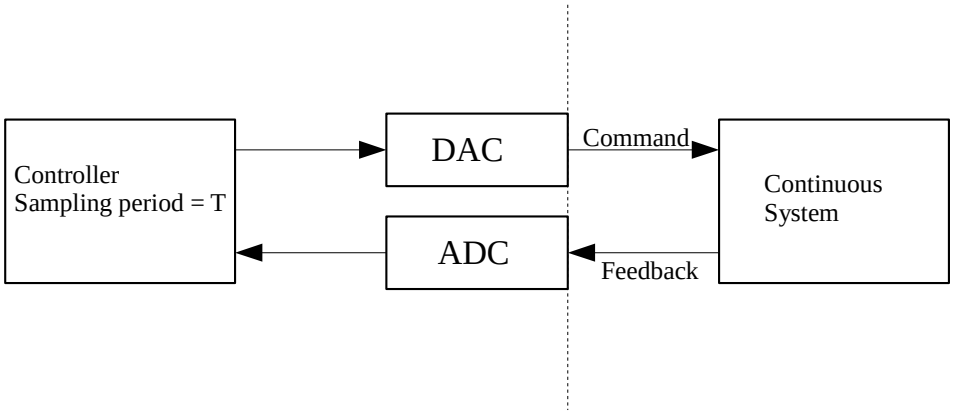

Figure 2.17: Real time control structure

The analog-to-digital converters (ADC) read the information of the sensors (accelerometer), and digital-to-analog converters (DAC) provide the control signal. Because the system has certain dynamics associated with it, the choice of the sampling period is important and it has to be related to the time constant of the physical system. Furthermore, if the sample time is constrained in duration by the time constant of the system, the control algorithm has to execute within that sample time. Each step of the control algorithm has to start exactly every sample time, and thus has to finish the computation within that, i.e. before the next step starts (Figure. 2.18) [30].

If the required computing time of a step is longer than the sample time, an

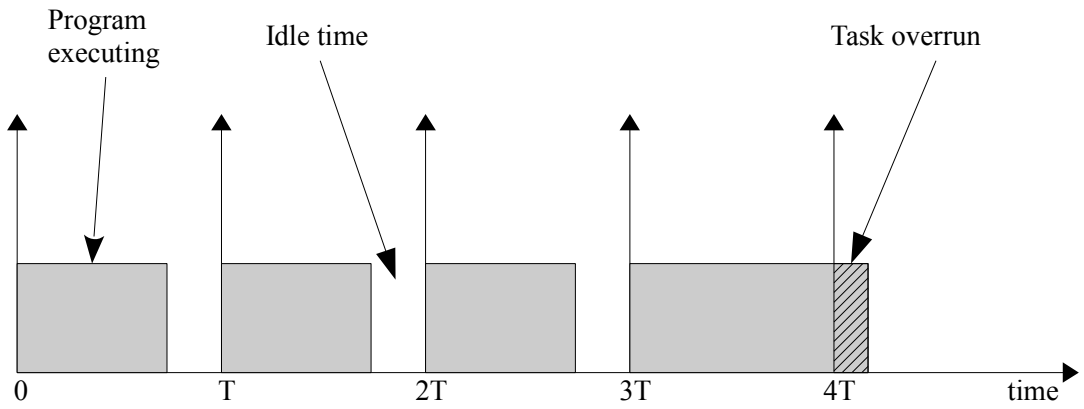

Figure 2.18: Real time control structure

overrun condition occurs and the control loop cannot run in real-time.
The general structure of a real-time program could be defined into tree main sections: initialization, the real-time tasks, and the background.
The initialization is for instruction that needs to be executed once, this part is usually at the beginning of program execution.
The real-time part is the task which is executed periodically based on the sample time. The real-time control program is executed in this part.
For this, inputs are read (e.g., from an ADC), control signals are computed, and vales are write on the outputs (e.g., with a DAC).
Finally, the last section is the background. This part includes the code that can be executed in the idle time, that is between the end of the real-time part execution and the start of the next step. [30]

According to the system transfer function, the signal bandwidth and the computational power limit, the sampling frequency chosen for the shaker control loop is $f_s = 5kHz$.

This page intentionally left blank.

Chapter 3

Feedforward control

3.1 Introduction

Adaptive filtering techniques have been successfully applied in many telecommunication problem, such as channel equalization, echo and interference cancellation, speech analysis and synthesis [31–34].
In this chapter is shown how adaptive control algorithms can be employed for controlling an unknown and time varying physical systems.
The physical system to be controlled, also called *plant*, may be unknown and could change its characteristics in the time.
However, some prior knowledge of the plant transfer function, like transient response and how fast the characteristics change, will be needed in order to establish proper adaptive control [16].
For a time-variant plant an adaptive control system would be advantageous than a controller with fixed parameters, since the first one can be iteratively adjusted to follow the unknown and time-variant response of the plant to be controlled.
In signal processing theory many problems are solved by adjusting weights of a transversal filter by minimizing a certain performance function, and employing the resultant adaptive filters for the system equalization or control, without using a direct feedback signal [35, 36].
In this chapter, the methodology of adaptive signal processing are used to solve the classic problems in adaptive control. The result is called *Adaptive Inverse Control*.

3.2 Adaptive inverse model control system

A conventional control system (Figure. 3.1), such as PID controller uses direct feedback. It compares the response of the plant with the desired signal, and uses the difference to drive the controller of the plant whit the aim to have the desired

signal at the output of the plant [37].
The difference between the plant output and the desired signal is the error signal. The error signal is then used by the controller, which amplifies and filters it to produce an appropriate driving signal for the plant in order to minimize the error.

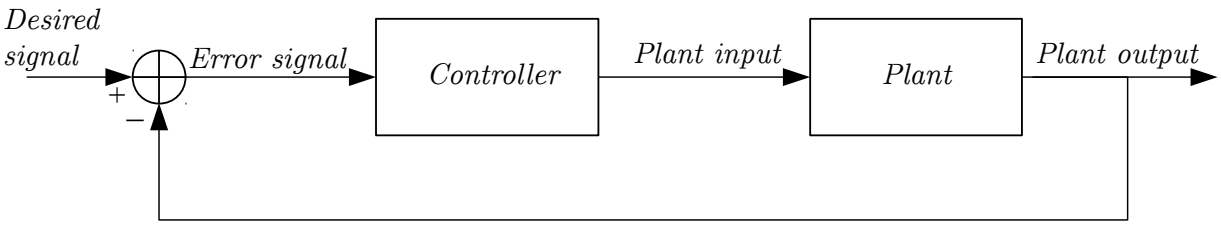

Figure 3.1: Conventional feedback control system

When the plant characteristics are time variable, it is sometime necessary to design the controller that follows the time changing dynamics of the system. But achieving this aim in classic adaptive control is usually complicated, moreover, risk to have an unstable control is high [38]. As explained in 1.2.3, when the plant is unknown, an identification iterative process can be used to estimate the plant transfer function, and the inverse of this characteristic can be used to control the plant.
The basic concept of the adaptive inverse control technique is to drive the physical system with a controller characterized by a transfer function calculated as the inverse of the systems one [39] (Figure. 3.2).

The target of this system is to cause the plant output follow the desired signal. Since the plant is unknown, an adaptive process of the controller parameters is required to iteratively achieve a better representation of the plant inverse.
The error signal calculated as difference between the plant output and the desired signal, is used by an adaptive algorithm for the adjustment of the controller in order to minimize power of the error signal.
The controller, in this application is composed of FIR filter having an input and an output. The controller is adapted by changing is filter coefficients by the adaptive algorithm, which is driven by the error signal. Comparing a conventional control system (Figure. 3.1) with a feed-forward controller (Figure. 3.2), minimizing the mean squared error is achieved in the first case by using the error signal to create the best driving signal for the plant, whereas, in the feed-forward case the error

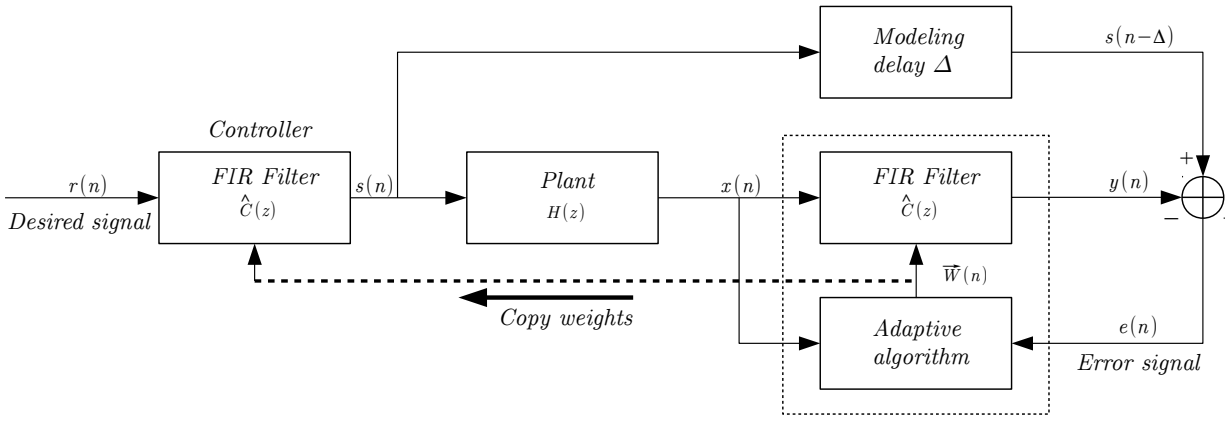

Figure 3.2: Adaptive inverse model control system

signal is used to evaluate a new array of coefficients for the controller, in order to reshape the desired signal, and is not fed back directly on the plant input.
In adaptive process, a small mean squared error, means that the controller has become a good inverse of the plant, at least in the band of the desired signal. Therefore, the cascade of the controller and plant would have a combined transfer function near the unity gain.
How discussed in 1.2.3 if the plant is non-minimum phase or has an internal delay, the inverse controller may have difficulty to match the inverse transfer function. A discrete delay line Δ is then necessary to match the inverse transfer function [16].

3.3 Time domain Feedforward control

3.3.1 Least Mean Squares algorithm

The least mean square (LMS) algorithm, which was first proposed by Widrow and Hoff in 1960, is the most widely used adaptive filtering algorithm [40]. Considering a N-weight transversal Wiener filter (Figure. 3.3), the time-dependent tap weights

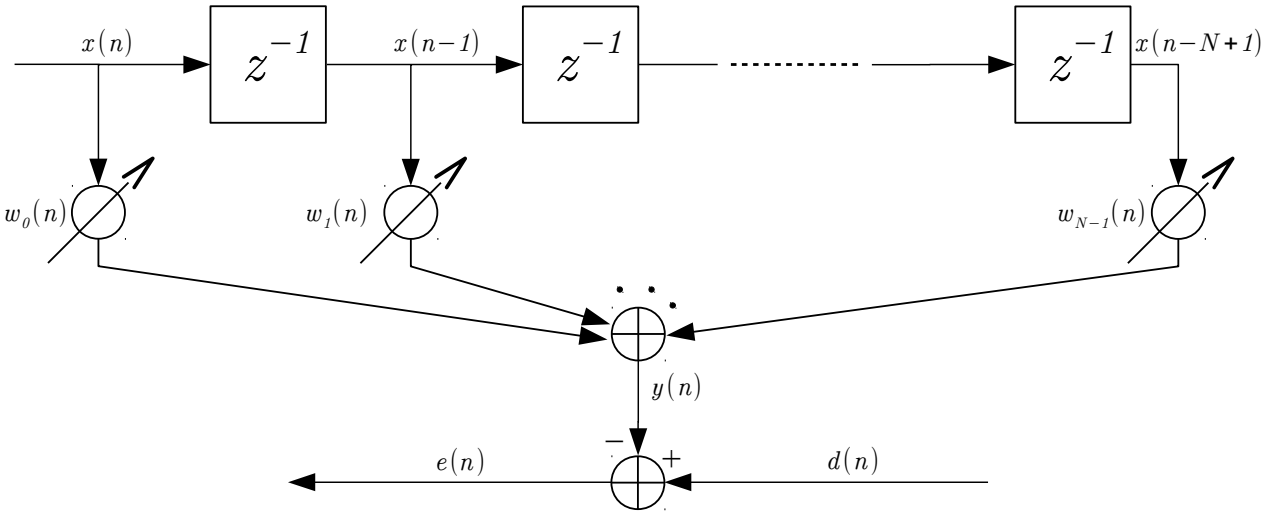

Figure 3.3: An N-weight transversal Wiener filter

$w_0(n), w_0(n), \ldots, w_{N-1}(n)$ are adapted in order that the error signal $e(n)$ (Eq. 3.5) is minimized in the mean-square sense, thus the name LMS. When the process $x(n)$ and $d(n)$ are jointly stationary, the LMS algorithm converges to a set of taps weight equal to the Wiener–Hopf solution, without explicitly solving the Wiener–Hopf equation [41].
The LMS algorithm is a stochastic implementation of the steepest-descent algorithm [42]. Considering the method of steepest descent, and assuming that all the signal involved are real-valued signal. The output of the transversal Wiener filter $y(n)$, can be calculated as product of the weights vector (Eq. 3.1) an the last N sample of the input signal (Eq. 3.2), as in (Eq. 3.3).

$$\vec{w} = [w_0, w_1, \ldots w_{N-1}]^T \tag{3.1}$$

$$\vec{x}(n) = [x(n), x(n-1), \ldots, x(n-N+1)]^T \tag{3.2}$$

$$y(n) = \sum_{i=0}^{N-1} w_i(n)x(n-i) \tag{3.3}$$

$$\vec{y}(n) = \vec{w}^T\vec{x}(n) \tag{3.4}$$

The same holds for the error signal and the performance function, respectively reported in (Eq. 3.5) and (Eq. 3.6), where E is the first order expectation function.

$$e(n) = d(n) - y(n) \tag{3.5}$$

$$\begin{aligned} \xi &= E[e^2(n)] \\ &= E[d^2(n)] - 2\vec{w}^T\vec{p} + \vec{w}^T R\vec{w} \end{aligned} \tag{3.6}$$

where:
$R = E[\vec{x}(n)\vec{x}^T(n)]$ is the autocorrelation matrix of the filter input.
$\vec{p} = E[\vec{x}(n)d(n)]$ is the cross-correlation vector between $\vec{x}(n)$ and $\vec{d}(n)$.

The performance function ξ is a quadratic function of the filter weights vector $\vec{w}$, and it has a single global minimum defined by the solution of the Wiener-Hopf equation (Eq. 3.7), were $\vec{w}_0$ is the optimal weights solution.

$$R\vec{w}_0 = \vec{p} \tag{3.7}$$

However, R and $\vec{p}$ are not available in many real time application. The basic idea of the steepest descent algorithm is to employ an iterative search method instead to trying to solve the Eq. 3.7 directly. Starting from an initial guess $\vec{w}(0)$ for the optimal solution $\vec{w}_0$, a recursive search method that require many iteration is used to converge to $\vec{w}_0$. Consider now the gradient of the performance function ξ in order to find its minimum, it is given by Eq. 3.8.

$$\nabla\xi = 2R\vec{w} - 2\vec{p} \tag{3.8}$$

With an initial guess of $\vec{w}_0$ at $n = 0$ the weights vector at he k-th iteration is denoted as $\vec{w}(k)$. The recursive Eq. 3.9 can be used as update rule for the $w(k)$.

$$\vec{w}(k+1) = \vec{w}(k) - \mu\nabla_k\xi \tag{3.9}$$

where $\mu > 0$ is called *step-size*, ∇ is the gradient operator (Eq. 3.10), and $\nabla_k\xi$ denotes the gradient vector $\nabla\xi$ evaluated for $\vec{w} = \vec{w}(k)$.

$$\nabla = \left[\frac{\partial}{\partial w_0}\frac{\partial}{\partial w_1}\cdots\frac{\partial}{\partial w_{N-1}}\right]^T \tag{3.10}$$

Substituting now (Eq. 3.8) in (Eq. 3.9) the update rule can be written as (Eq.3.11).

$$\vec{w}(k+1) = \vec{w}(k) - 2\mu(R\vec{w}(k) - \vec{p}(k)) \tag{3.11}$$

The convergence of $\vec{w}(k)$ to the optimum solution $\vec{w}_0$ and the convergence spread are function of the step-size parameter μ. A large step-size may result in divergence of this recursive equation. In order to evaluate the convergence process of $\vec{w}(k)$ to the optimum solution $\vec{w}_0$, (Eq. 3.11) can be re-arranged as (Eq. 3.12) by (Eq. 3.7).

$$\vec{w}(k+1) = (1 - 2\mu R)(\vec{w}(k) - \vec{w}_0) \tag{3.12}$$

Defining the vector $\vec{v}(k)$ as (Eq. 3.13), then (Eq. 3.12) can be written as (Eq. 3.14).

$$\vec{v}(k) = \vec{w}(k) - \vec{w}_0 \tag{3.13}$$

$$\vec{v}(k+1) = (I - 2\mu R)\vec{v}(k) \tag{3.14}$$

Where I is the N-by-N identity matrix. Considering now the auto-correlation matrix R, it may be diagonalized by using a unitary similarity decomposition (Eq. 3.15).

$$R = Q\Lambda Q^T \tag{3.15}$$

Where Λ is a diagonal matrix consisting of the eigenvalues $\lambda_0, \lambda_1, \ldots, \lambda_{N-1}$ of R, and Q is a matrix with corresponding orthonormal eigenvectors in its columns. Substituting (Eq. 3.15) in (Eq. 3.14) and replacing I with QQ^T we get (Eq. 3.16):

$$\begin{aligned} \vec{v}(k+1) &= (QQ^T - 2\mu Q\Lambda Q^T)\vec{v}(k) \\ &= Q(I - 2\mu\Lambda)Q^T\vec{v}(k) \end{aligned} \tag{3.16}$$

Premultiplying (Eq. 3.16) by Q^T and denote $\vec{v}'(k)$ as (Eq. 3.17), we obtain a simplified recursive equation in terms of $\vec{v}'$ (Eq. 3.18).

$$\vec{v}'(k) = Q^T\vec{v}(k) \tag{3.17}$$

$$\vec{v}'(k+1) = (I - 2\mu\Lambda)\vec{v}'(k) \tag{3.18}$$

The vector recursive Eq. 3.18 can be separated into scalar recursive equation (Eq. 3.19), where $v_i'(k)$ is the ith element of the vector $\vec{v}'(k)$.

$$v_i'(k+1) = (1 - 2\mu\lambda_i)v_i'(k) \tag{3.19}$$

for $i = 0, 1, \ldots, N-1$

Starting with a set of initial values $v'_0(0), v'_1(0), \ldots, v'_{N-1}(0)$ and iterating (Eq. 3.19) k times, we get (Eq. 3.20).

$$v'_i(k) = (1 - 2\mu\lambda_i)^k v'_i(0) \tag{3.20}$$

for $i = 0, 1, \ldots, N-1$

The equation (Eq. 3.20) implies that $\vec{v}'(k)$ can converges to zero if and only if the step-size parameter μ is selected so that :

$$|1 - 2\mu\lambda_i| < 1 \tag{3.21}$$

for $i = 0, 1, \ldots, N-1$

That is, $0 < \mu < \frac{1}{\lambda_i}$ for all i or equivalently $0 < \mu < \frac{1}{\lambda_{MAX}}$, where λ_{MAX} is the maximum of the eigenvalues $\lambda_0, \lambda_1, \ldots, \lambda_{N-1}$.

Many studies in literature prove that the best value for μ can be obtained as (Eq. 3.22) [34]. Moreover, the steepest-descent algorithm convergence is strictly related to the eigenvalues of the correlation matrix R . In other words, the performance of the steepest-descent algorithm depends to the power spectral density of the input signal, a weak excitation degrades the performance of the steepest-descent algorithm.

$$\mu_{opt} = \frac{1}{\lambda_{min} + \lambda_{max}} \tag{3.22}$$

How previously said, for the LMS algorithm, the steepest-descent cost function $\xi = E[e^2(n)]$ is replaced by is instantaneous coarse estimation $\hat{\xi} = e^2(n)$. Substituting $\hat{\xi} = e^2(n)$ in the steepest-descent recursion (Eq. 3.9) and replacing the iteration index k by the time index n we obtain (Eq. 3.23).

$$\vec{w}(n+1) = \vec{w}(n) - \mu\nabla e^2(n) \tag{3.23}$$

Note that the $i-th$ element of the gradient vector $\nabla e^2(n)$ is (Eq. 3.23),

$$\frac{\partial e^2(n)}{\partial w_i} = 2e(n)\frac{\partial e(n)}{\partial w_i} \tag{3.24}$$

Substituting $e(n)$ by (Eq. 3.5), and noting that $d(n)$ is independent of w_i, we obtain (Eq. 3.25):

$$\frac{\partial e^2(n)}{\partial w_i} = -2e(n)\frac{\partial y(n)}{\partial w_i} \tag{3.25}$$

Substituting for $y(n)$ from (Eq. 3.3) we get (Eq. 3.26).

$$\frac{\partial e^2(n)}{\partial w_i} = -2e(n)x(n-i) \tag{3.26}$$

Therefore, (Eq. 3.26) can be written in vector as (Eq. 3.27);

$$\nabla e^2(n) = -2e(n)\vec{x}(n) \tag{3.27}$$

Where $\vec{x}(n)$ is (Eq. 3.2).

Substituting this result in (Eq. 3.23) we get the LMS recursive equation (Eq. 3.28).

$$\vec{w}(n+1) = \vec{w}(n) + 2\mu e(n)\vec{x}(n) \tag{3.28}$$

Equation (Eq. 3.28) represents the recursive updating rule of the filter coefficients at every sampling time.
The computational cost for every sampling time is of $2N$ additions, $2N+1$ multiplications, N multiplications for the output calculation $y(n)$, one for $2\mu e(n)$ and N multiplication for $2\mu e(n)\vec{x}(n)$.

3.3.2 LMS - Computer simulation

The validity and the performance of the adaptive control shown in Figure 3.2, are now verified through computer simulations. All the simulation results, which are given in the following have been generated by using MATLAB environment of MathWorks.

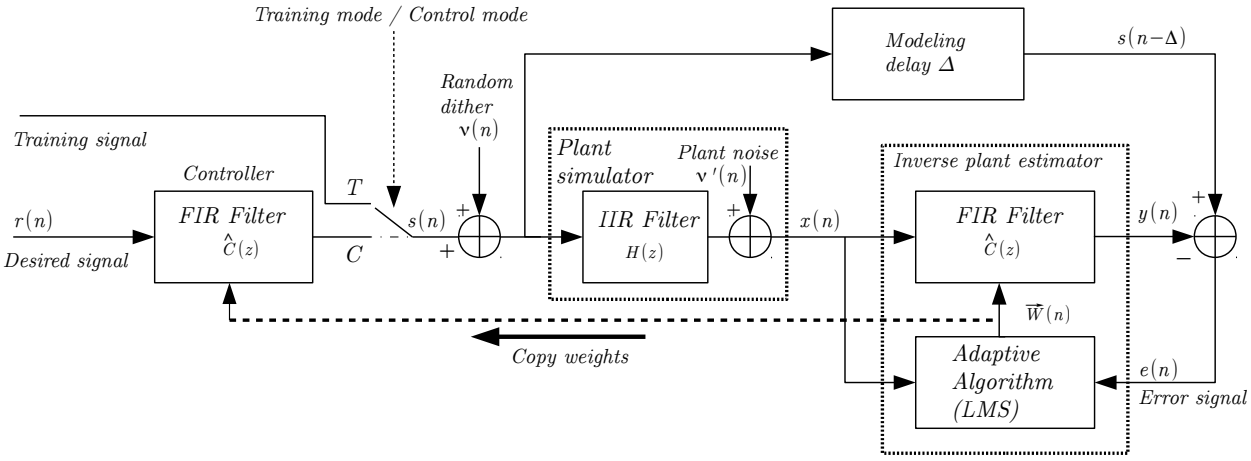

Figure 3.4: Adaptive inverse model control system with training

The system that was simulated is shown in Figure 3.4. It is a more realistic version of the control system depicted in Figure 3.2.
A small amplitude random dither signal $\nu(n)$ is introduced into the plant input $s(n)$.

A small injection of random noise in this point is useful to ensure that the adaptive modelling process will continue to keep the inverse model current, regardless of the reference signal is present. However, if the dither is necessary in many case in order to keep the adaptive process excited [17], it does disturb the plant and introduce noise in to the output.
The simulation use both a discrete time-time plant and a discrete-time controller. The plant transfer function $H(s)$ is simulated through an IIR filter, whose coefficients are calculated by a bilinear transformation of the plant transfer function extracted in chapter 2.
Since the acceleration sensor noise shows up at the plant output, the effect is called *Plant noise* $\nu'(n)$, and it is represented as an additive white Gaussian process with variance $\sigma^2 = 0.001$ added to the IIR filter output.
The controller is implemented as an N-tap transversal filter. Furthermore, a *Training / Control* switch is introduced on the plant simulator input for the training of the controller.
When the starting set of shared weights $\vec{W}(n)$ is equal to zero, the output of the FIR filter used as controller is also zero, and a training period allows to the inverse plant estimator to converge faster to a solution. In fact, without a training period at the beginning of the experiment, the inverse plant estimator results exited only by the small random dither $\nu(n)$, and according to the theory, it takes more time to converge.
The training signal $z(n)$ is generated by passing a unit variance white Gaussian sequence through an high order band pass filter, in order to limit the spectrum in the band of the system.
In this simulation the system is automatically switched in control mode after 50000 samples in time sequence. During this period, there was enough time for modelling of the inverse plant.
For this simulation the reference signal $r(n)$ was also generated at the same way of the training signal $z(n)$ in the defined bandwidth of interest $5 - 200Hz$ (Figure 3.5). Figure 3.6 shows the adaptive control time evolution.
Figure 3.5 shows a comparison of the plant output and the reference signal delayed of Δ samples (in order to make possible the graphical comparison) at the beginning of the simulation.
The inverse estimator has not yet converged, and an overall error occur, moreover the output noise contributes at the total error.
The second plot of Figure 3.6 shows the entire evolution of the MSE.
The inverse plant estimator has learned its function after the first 10 seconds.
The minimum mean squared error (MSE) is the metric used to quantify how well control is, a small value of MSE in indicate that the controller has converged, vice versa a large MSE in the steady state usually indicates the impossibility for the

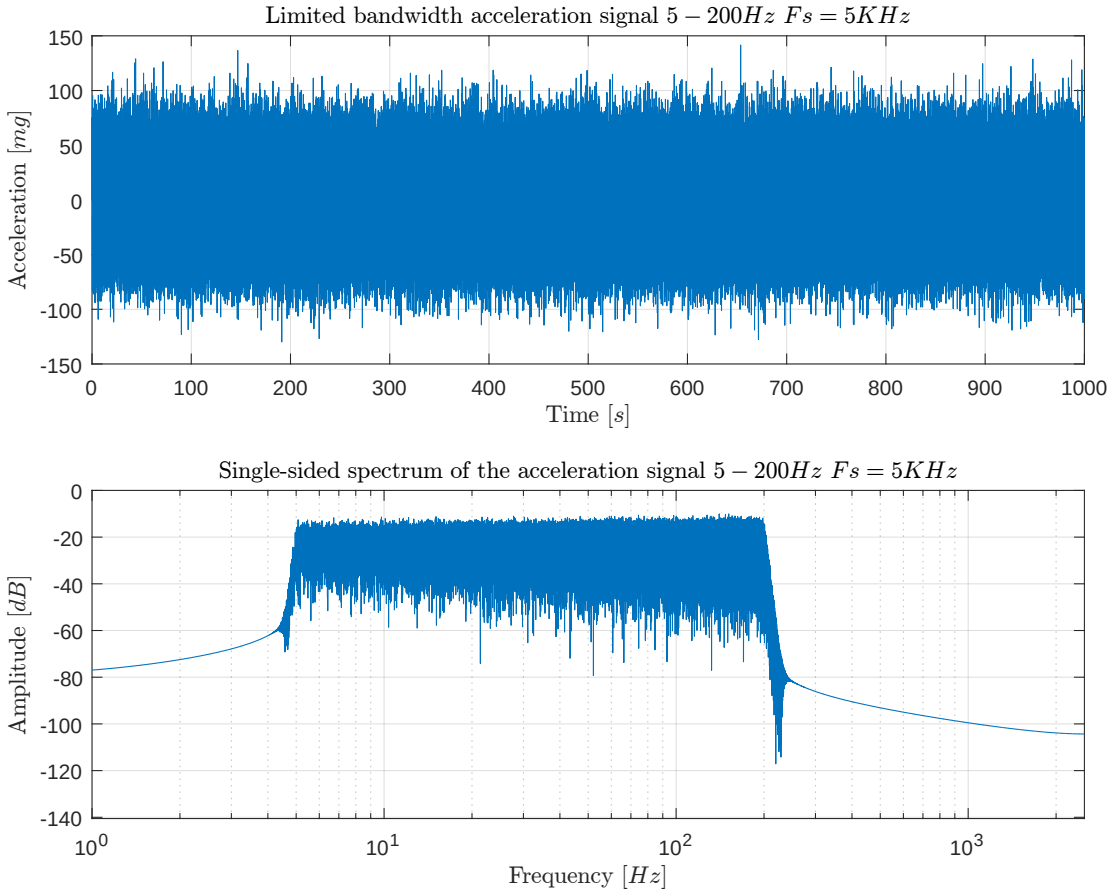

Figure 3.5: Limited bandwidth noise used for both reference and training signals

controller to model the plant [18]. Error persists, however, because of the plant noise.
The training mode is turned on 10 seconds after the start of the simulation, and turned off after other 10 second (50000 samples), in this time the error is reduced considerably.

Figure 3.8 shows the plant output and the delayed reference signal over the last part of the simulation. Tracking between them is definitely good, except for the small effects of the plant noise. In this simulation, the LMS algorithm does not converge for $\mu = \mu_{max} \approx 0.5$. The convergence behavior for $\mu = 0.03$ and $\mu = 0.3$ are illustrated through the learning curves (Figure 3.9).
How we can see a small value of μ cause a low convergence speed, however, a low convergence factor can reach a lower MSE asymptotically.
In the simulations the starting value for all coefficients is zero.

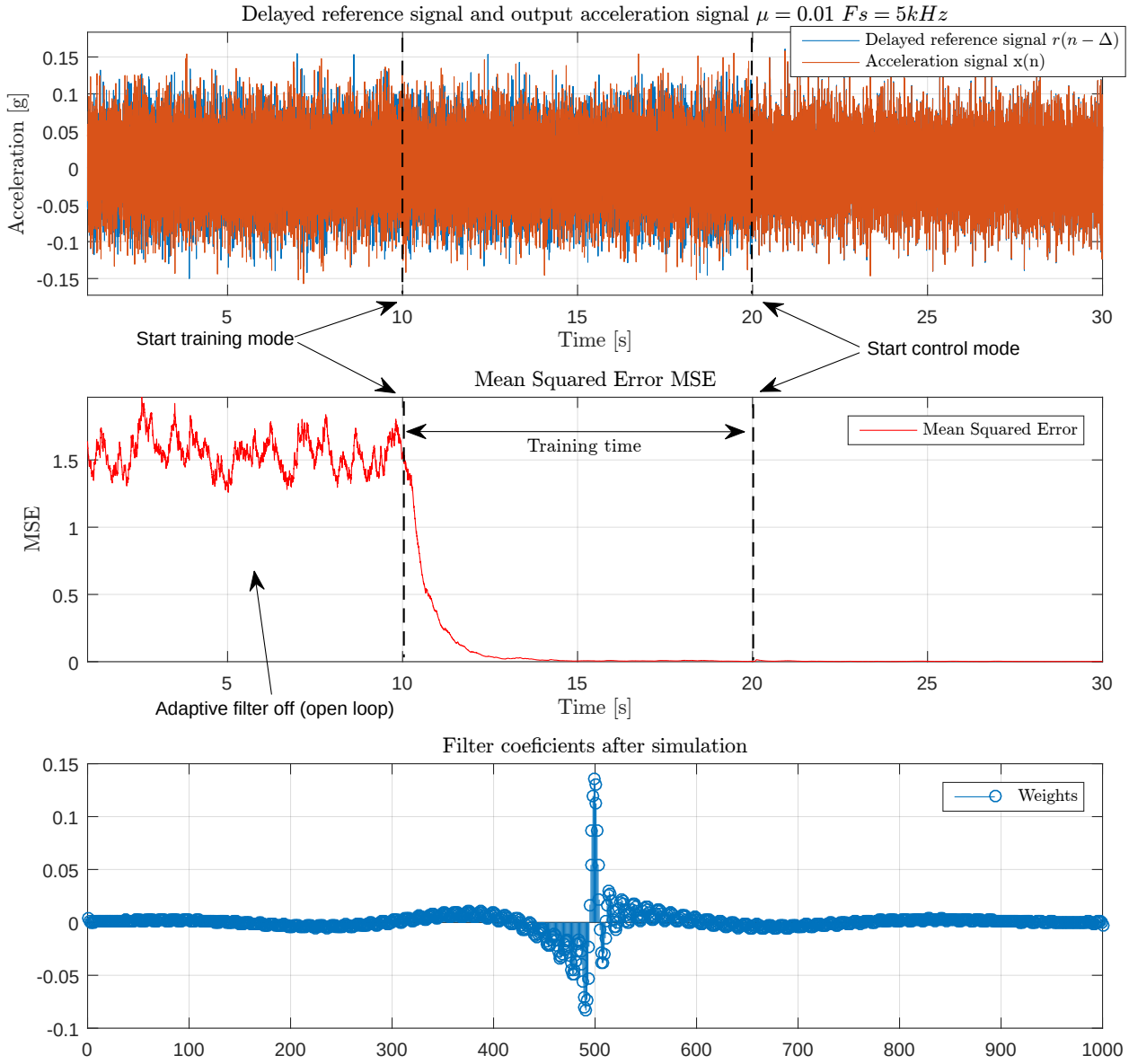

Figure 3.6: Matlab simulation of the overall system, training and control mode.

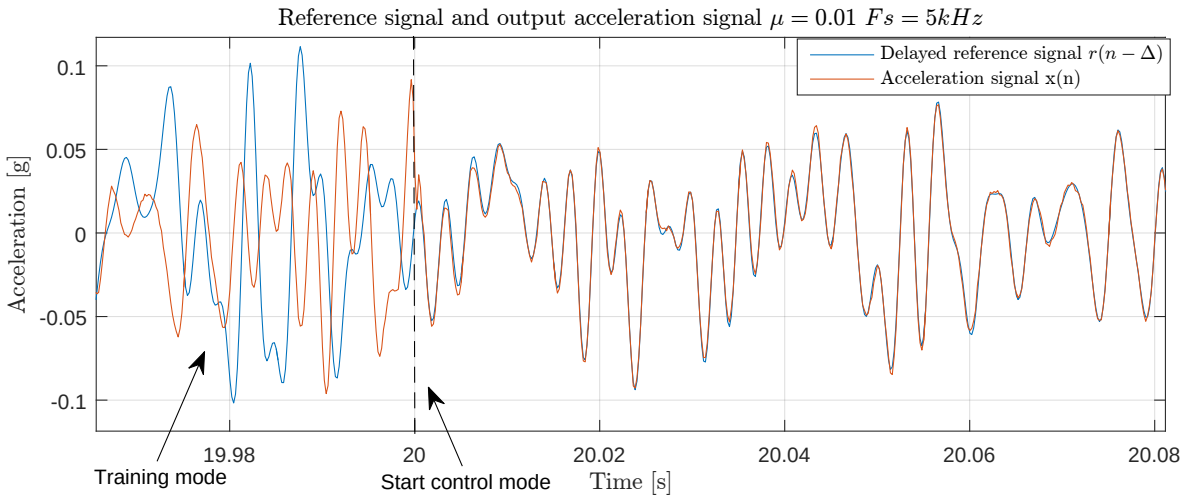

Figure 3.7: Training mode and control mode transition

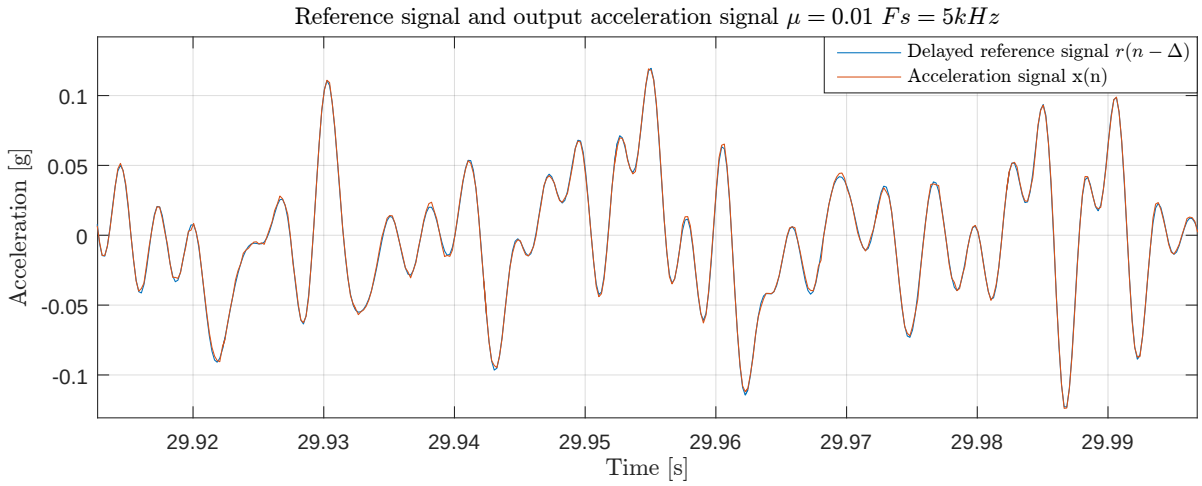

Figure 3.8: Steady state of the control mode

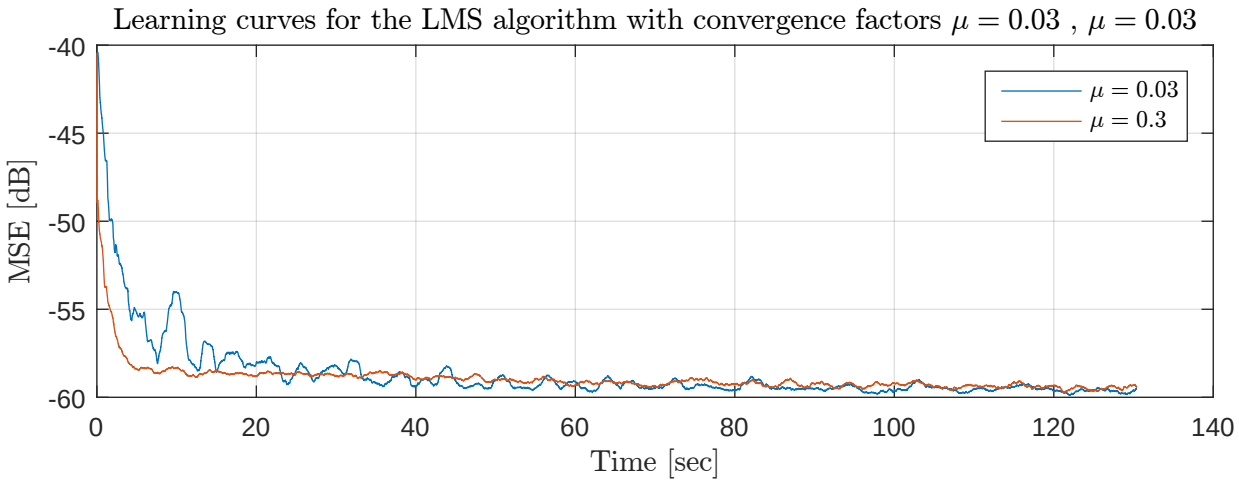

Figure 3.9: Learning curve for different convergence factor

3.4 Computational complexity

The computational load provided by the execution of the LMS algorithm is basically due to the multiplications needed for the parameters calculation and for the output signal calculation [43].
In this thesis the conventional LMS algorithm is uses for both simulation and real implementation.
How previously said, the computational cost for every sampling time is of $2N$ additions, $2N + 1$ multiplications, N multiplications for the output calculation $y(n)$, one for $2\mu e(n)$ and N multiplication for $2\mu e(n)\vec{x}(n)$.
In control application depicted in Figure 3.4, another 2N additions and 2N multiplications for the FIR filter used as controller has to be included in the computational account.

Chapter 4

Implementation and practical results

4.1 Introduction

This chapter depicts the experimental evaluation (implementation) of the adaptive inverse control algorithm using dSPACE and Real Time Workshop. The control algorithm is developed using Simulink and implemented in real-time by using the dSPACE 1104 and its real-time interface library (RTI).
The Simulink software is used to develop the controller block diagrams, and the real time workshop to convert the Simulink model in C code.
The C code is then compiled and flashed on the dSPACE 1104. The driving signal, open loop response, closed loop response, and acceleration signal acquired from dSPACE Control Desk are observed in real time. The results of the simulations and the experimental results are compared. The experimental study demonstrated good closed loop performance and an acceptable computational load.

4.2 Control loop for a sine sweep

The sine sweep test is the first experimental test implemented on the real hardware. The dSPACE 1104 board is used here as the hardware controller level to connect the testing environment to the computer. A Simulink scheme was designed and implemented that makes use of ControlDesk to interact with the dSPACE board. The complete Simulink implemented model for sine sweep is shown in Figure 4.9. Mainly, it consists of two parts, specifically the reference signal generator and the controller loop. The reference signal generation section is shown in Figure 4.1. This section is basically composed by two independent signal generator and an output selector. The fist signal generator is used in the training mode, it is

a limited bandwidth noise generator realized through an uniformly distributed random number generator followed by a high order IIR band-pass filter. The output signal of the IIR filter is used in the training mode in order to excite the complete band of interest (Figure 4.2), and cause the convergence of the inverse plant estimator.

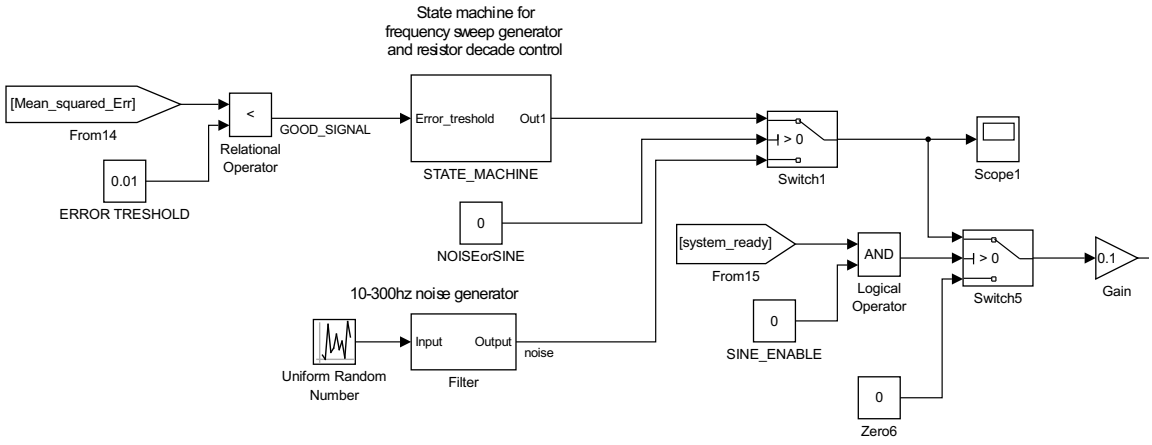

Figure 4.1: Simulink model for reference signal generation section

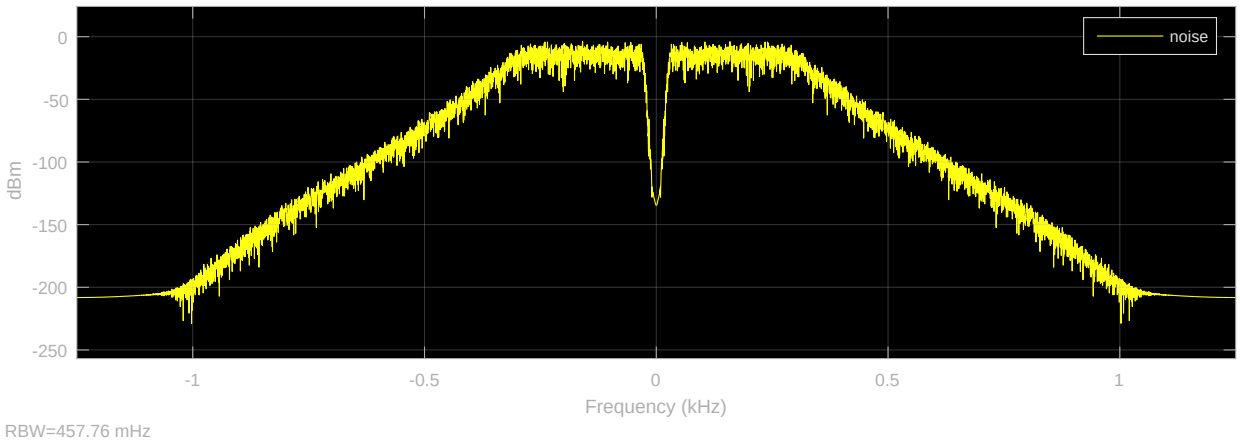

Figure 4.2: Spectrum of the limited bandwidth noise used in training mode

The second signal generator is the sine-dwell source. Sine-dwell signal is the discrete version of a sine sweep. The frequency is not varied continuously but is incremented by discrete amounts at discrete time points. Mathematically, for the rth time interval, the dwell signal is (Eq. 4.1) with $T_{r-1} \leq t \leq T_r$,

$$r(t) = A\sin(2\pi f_r t + \phi_r) \tag{4.1}$$

in which f_r, A, and ϕ_r are kept constant during the time interval T_{r-1}, T_r.
The frequency increments can be constant or increasing with the sweep time (exponential sweep). In the exponential sweep the the dwelling-time have an inverse proportional relation the frequency. In fact, when the frequency increase the number of period that occur during a given time also increase, and the steady-state condition occurs early [44].
The sine-dwell signal source was achieved through a programmable state machines (Figure 4.3) properly configured in order to manage the sine frequency evolution and the sweep duration. In order to automatize some typical energy harvesting measurements, the state machines include also the control of an external variable resistive load usually employed to evaluate the generator power output during the frequency sweep [45]. The follow table shows a brief description of the input and output signal of the state machine.

Input and output description	
Input	Description
start	Boolean, start state machines
stop	Boolean, stop state machines
Max_Freq	Maximum frequency in the sweep $[Hz]$
Min_Freq	Minimum frequency in the sweep $[Hz]$
t_hold_res	Retention time for every resistance value $[s]$
R_sweep_enable	Boolean, activate or deactivate the resistance sweep function
low_res	Minimum value in the resistance sweep $[ohm]$
step_res	Define the step-size in the resistance sweep $[ohm]$
high_res	Maximum value in the resistance sweep $[ohm]$
direction_R	Boolean, define the resistance sweep direction, high to low or low to high
Error_TH	Boolean, pause the state machine if the MSE is higher than a threshold
step_freq	Define the step-size in the frequency sweep $[Hz]$
t_hold_freq	Retention time for every frequency value $[s]$
direction_F	Boolean, define the frequency sweep direction, high to low or low to high
cycle_en	Boolean, enable the exponential sweep mode (constant number of cyle)
n_cycle	Number of cycle in the exponential sweep mode
zc_trig	Boolean, signal to the state machine the zero crossing of the sine wave
pause	Boolean, pause the state machines
single_freq	Boolean, disable the sweep mode
s_freq_in	Define the fixed frequency value in no-sweep mode $[Hz]$
Output	Description
driving_Freq	It is the current frequency value for the sine wave $[Hz]$
gain	It is a multiplicative gain for the sine wave
valid_measure	Boolean, it indicates when the error is below the threshold
resistor	Is the current resistor value for the resistance sweep $[ohm]$
set_freq	Boolean, it is true when a new frequency value has to be set
F'hold_time	Indicates the duration of the current frequency $[s]$

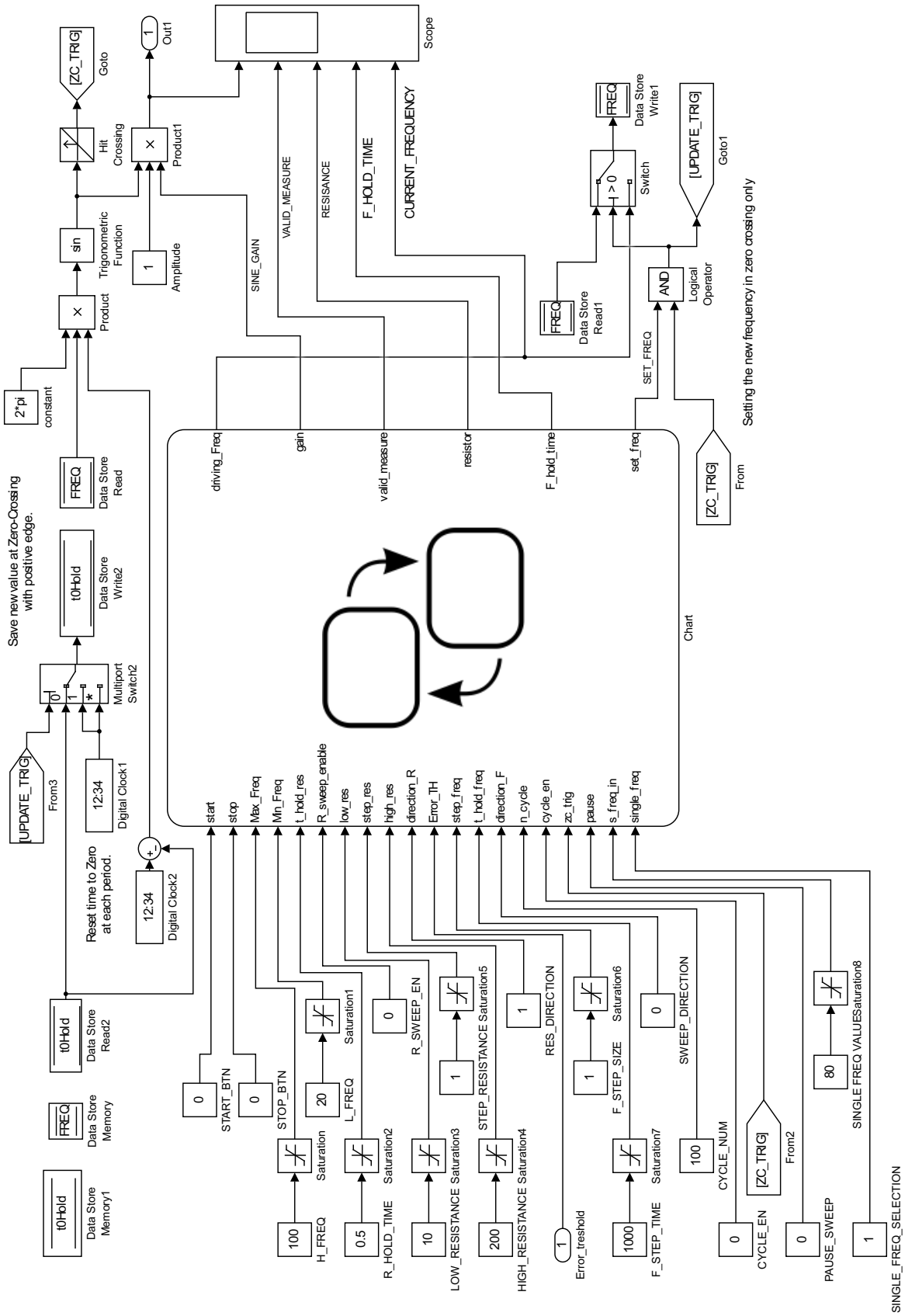

Figure 4.3: Sine-dwell signal generator achieved by a state machine

After the signal generation section, the reference signal is directly sent to the controller section (Figure 4.4). How explained in chapter 3.3.2 a *Training/Control* selector choose the driving signal for the plant in agreement with the current mode. The interfacing with the plant is shown in Figure 4.5. In this model the acceleration

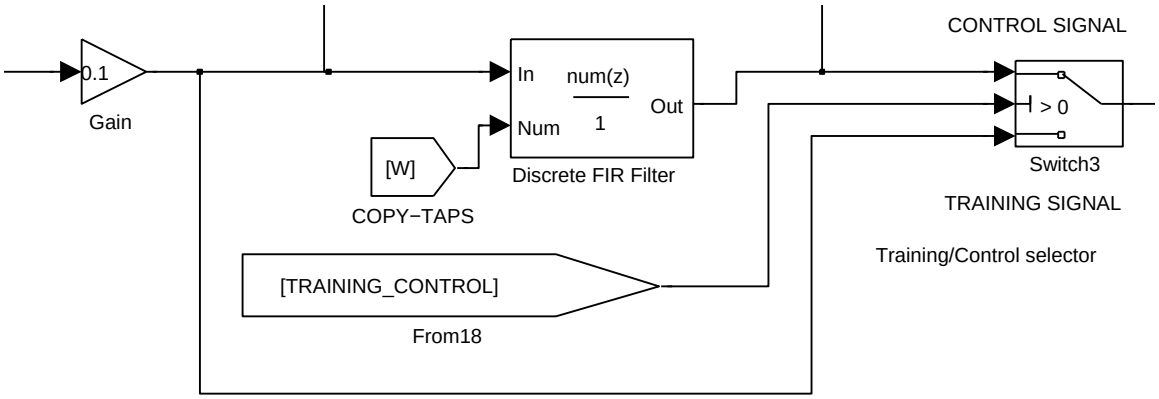

Figure 4.4: Controller section and mode selector

signal is provided by DS1104MUX_ADC got from the dSPACE library, it converts the analog acceleration signal in to digital one. The analog driving signal is fed to the plant through the DS1104DAC_C1 block that converts the digital into analog signal. This two blocks allow to connect the external analog devices to the Simulink model and close the whole control loop.

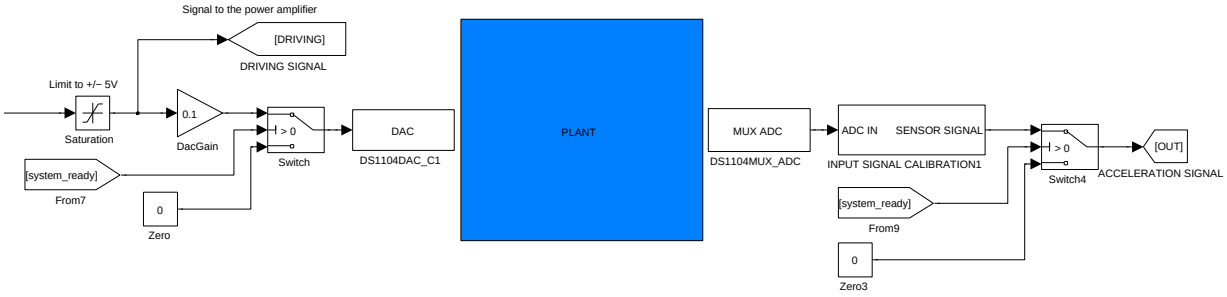

Figure 4.5: Plant inteterface

Figure 4.6 shows the main part of the control system, that is the inverse plant estimator. A delayed version of the plant driving signal is directly sent to the inverse plant estimator as desired signal. The inverse plant estimator (implemented as a Matlab function) compares the desired signal with the measured acceleration signal, and iteratively calculates the best filter coefficients in order to match the

desired signal. The coefficients are then copied to the FIR filter used as controller (Figure 4.4).

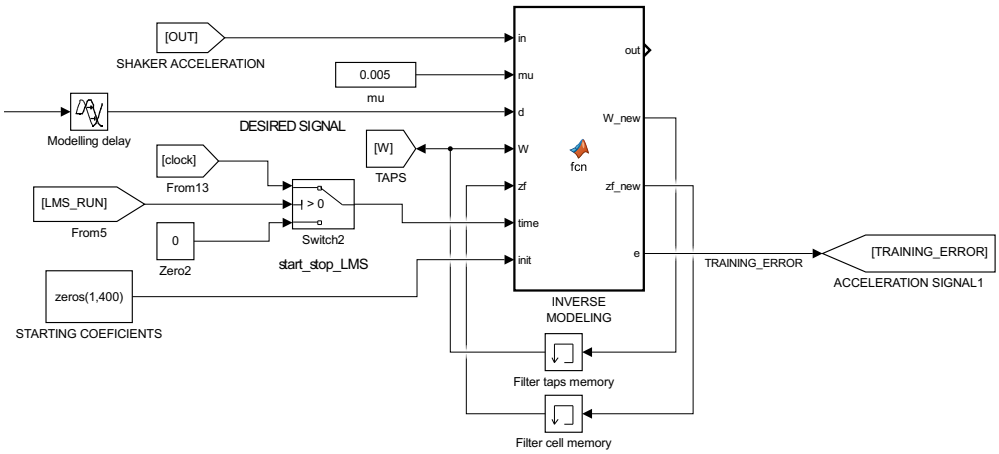

Figure 4.6: Inverse model estimator

In order to manage the sweep generator, the variable resistor load and the whole loop, a ControlDesk interface has been built up and used to interact with the dSPACE board (Figure 4.7).

Figure 4.10 shows the time sequence of a typical sine-dwell experiment performed on the real system (Figure 4.8) recorded by ControlDesk. We can notice that during the sweep experiment the MSE error remains quite low, this means that the real-time control loop is working well.

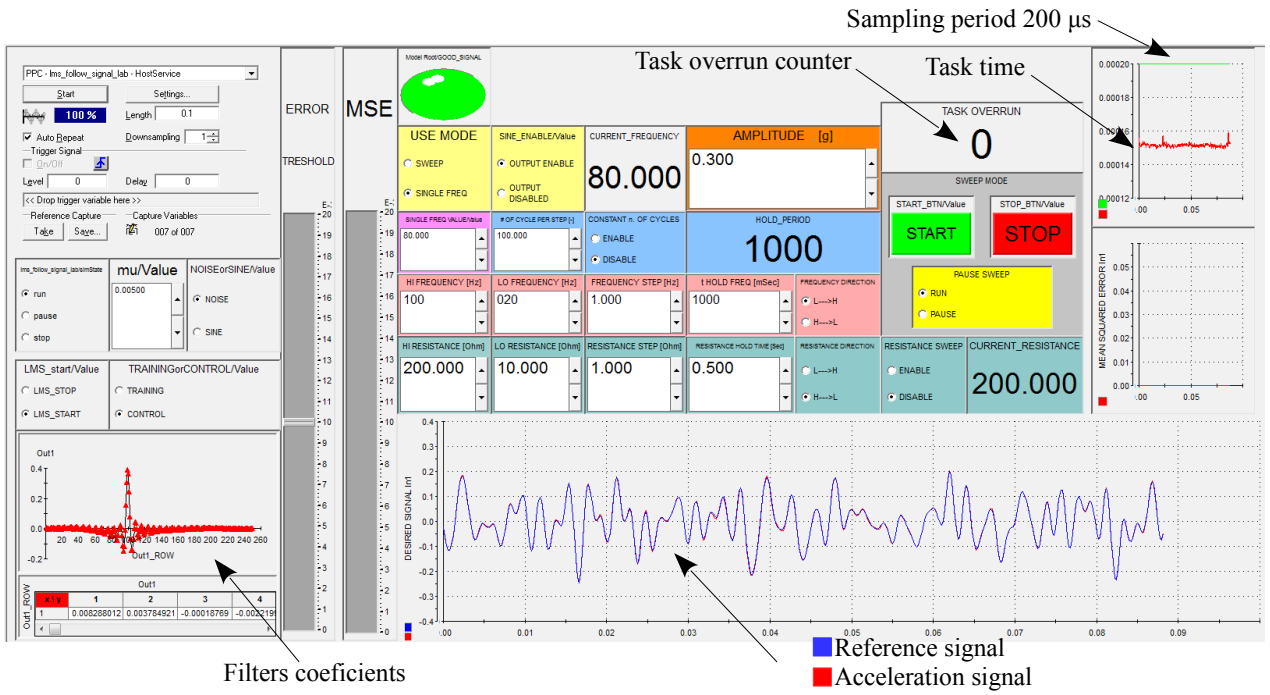

Figure 4.7: ControlDesk interface used to interact with dSPACE board (training mode)

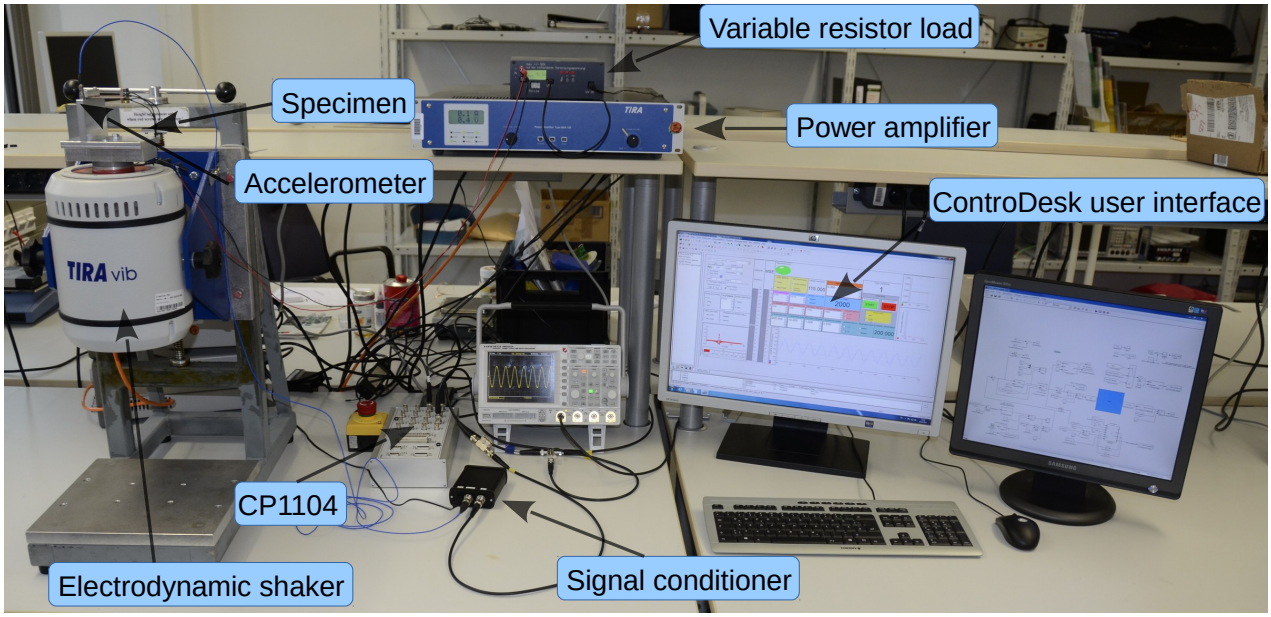

Figure 4.8: Laboratory set-up used for energy harvesting experiments

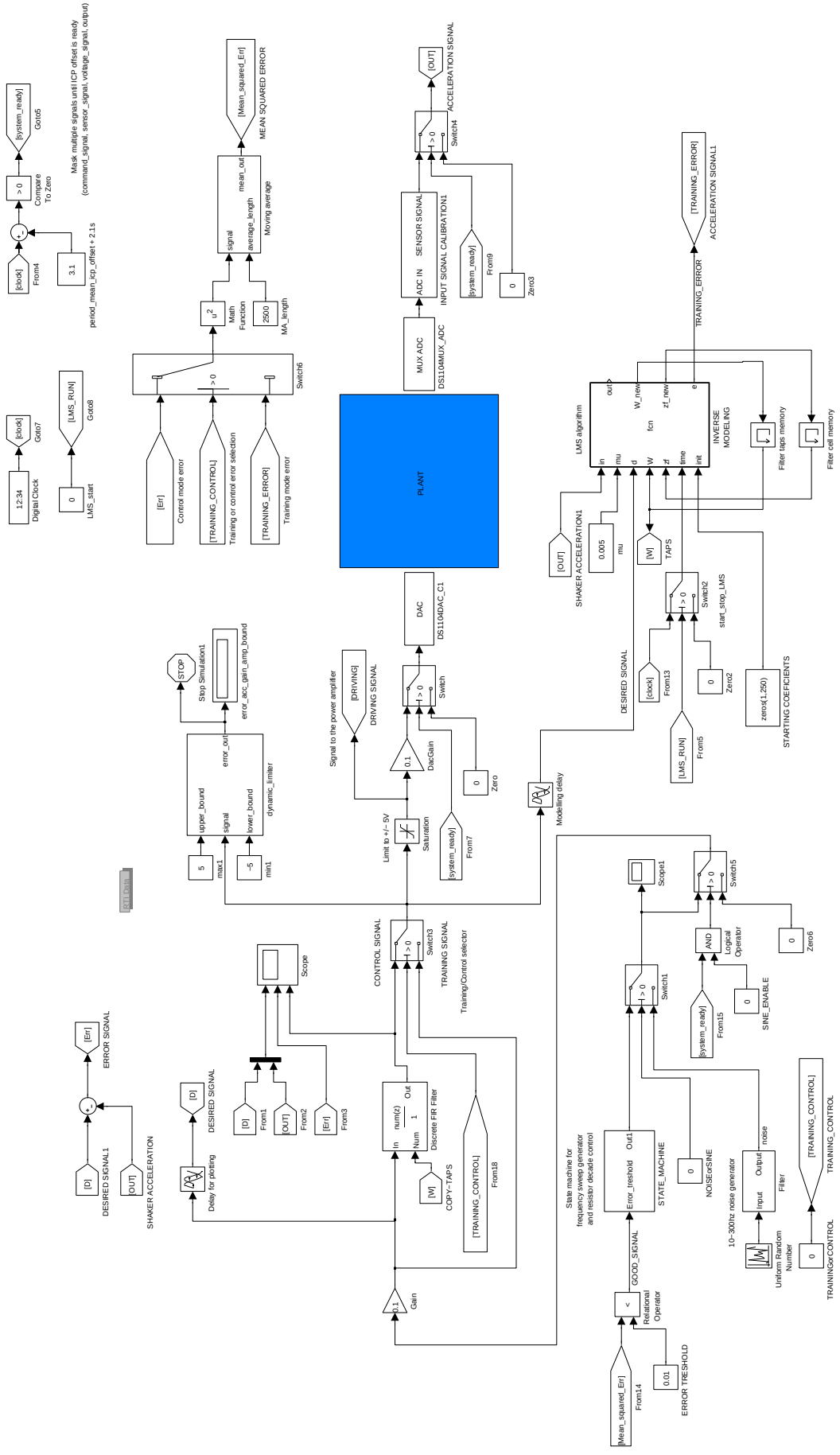

Figure 4.9: Simulink model for sine-dwell test and control loop

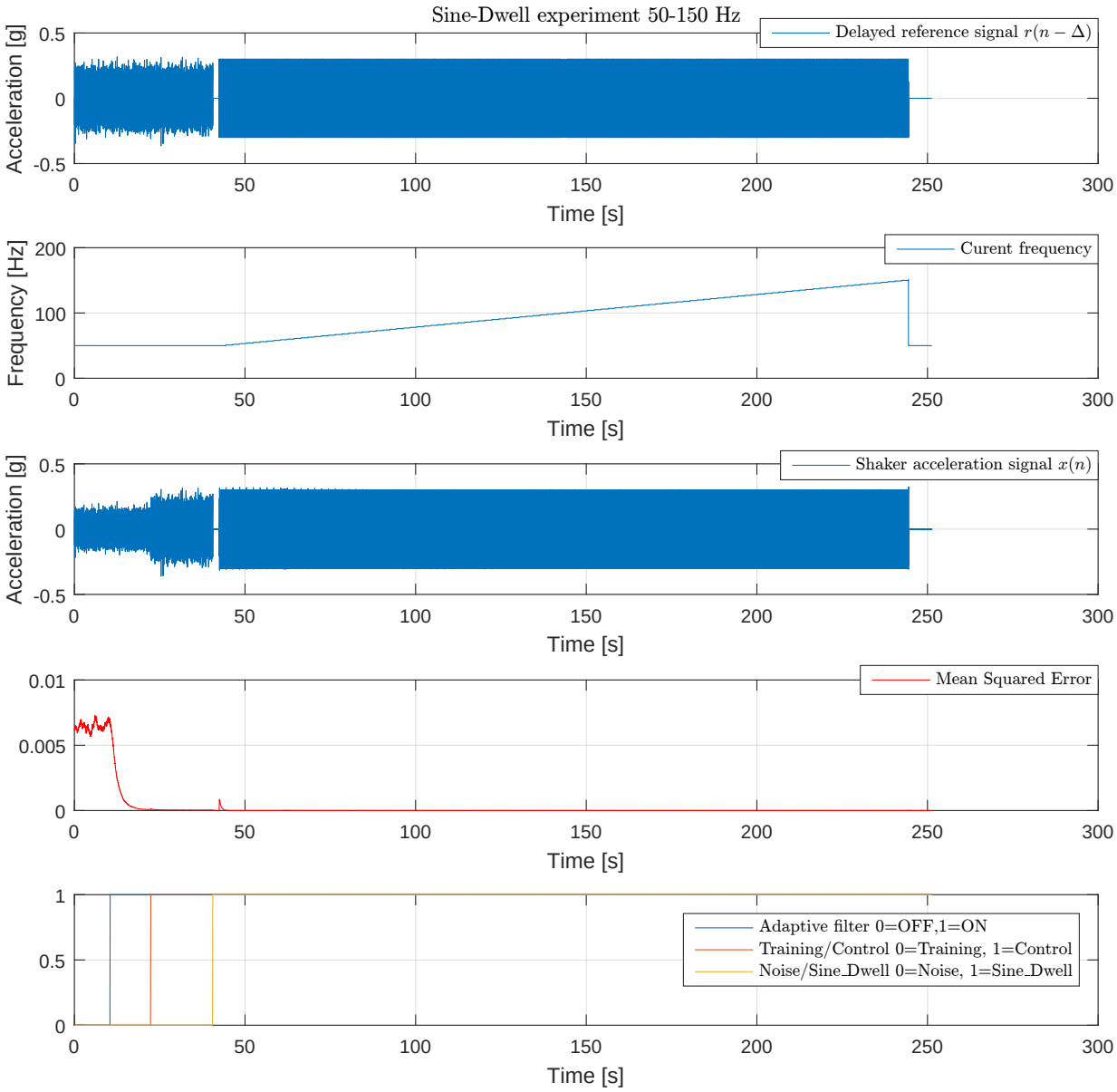

Figure 4.10: Evolution of the signals in a real sine-dwell vibration test

4.3 Control loop for pre-recorded signal

Recorded measurement data such as acceleration of real environment must be played back on an HIL system. These signal behaviors are easy to introduce into test scenarios, as they are not integrated into the simulation model, but are added dynamically during run time with Real-Time Testing. It can be easily replayed via ControlDesk by loading the data in the dedicated stimulus editor. The simulation model therefore remains independent of individual test cases. Figure 4.11 shows signal generation section for the real vibration test. The *TA Replace* block, from the dSPACE RTI library, is used to substitute the noise signal whit the pre-recorded signal loaded by the ControlDesk stimulus editor. The *TA SubControl* block, represents the control interface for the *TA Replace* block. The remaining part of the control loop is exactly the same of the sine-dwell layout.

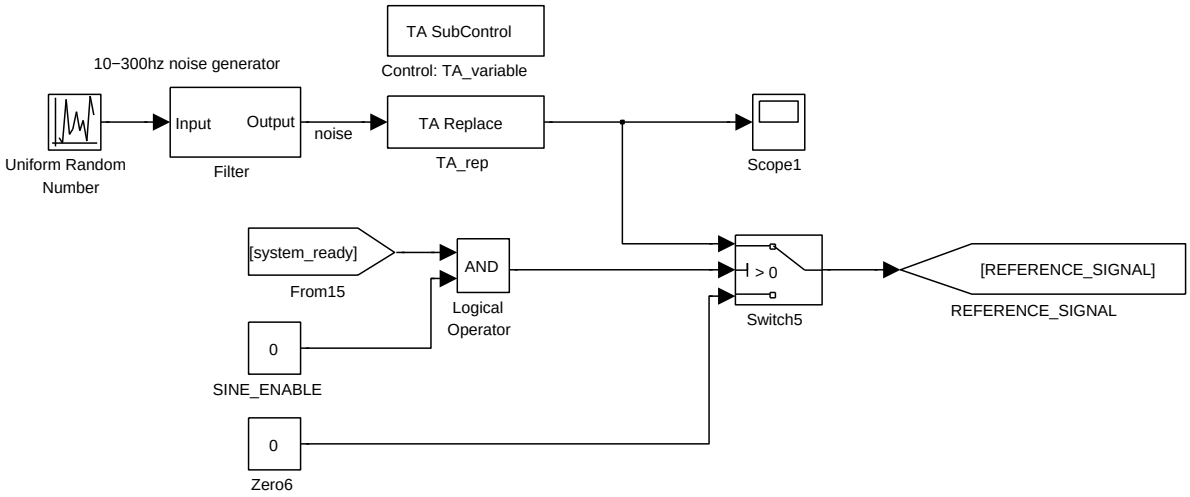

Figure 4.11: Reference signal generation section for rela vibration

Figure 4.12 shows the time evolution of an environmental test performed on the real system (Figure 4.8) recorded by ControlDesk. The environmental vibration signal (starting around $t = 26s$) was recorded during an airplane landing. Also in this case we can notice that during the experiment the MSE error remains quite low, this means that the real-time control loop is working well, and a real vibration scenario can be reproduced in laboratory with a low error.

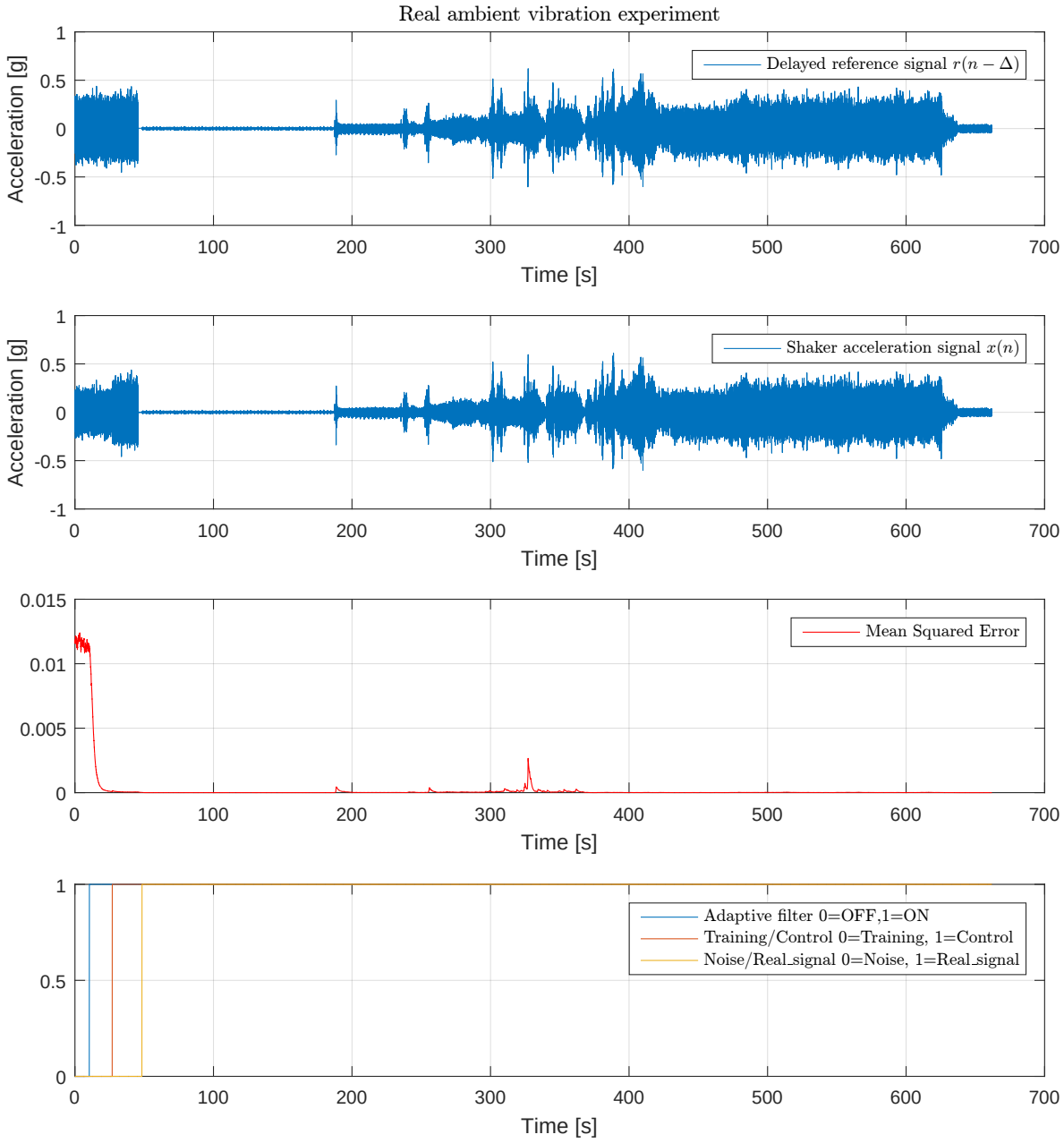

Figure 4.12: Evolution of the signals of a real environmental vibration test

Chapter 5

Conclusion and further developments

A theoretical, simulative, and practical assessment of the shaker real time control system has been conducted in this thesis. The vibration tests used the electrodynamic shaker as exciter. The control algorithm have been implemented using the dSPACE DS1104 power PC. Modelling and analysis of the shaker dynamics and control algorithm was simulated in MATLAB/Simulink. The practical has been executed in real-time with Simulink model and HIL block library on the dSPACE DS1104 using ControlDesk to real time interaction. To compensate for the uncertainty imposed by the shaker and specimen dynamics, a time domain adaptive control has been chosen as the best method achieve the control objective. The time domain adaptive filtering method was used to compute the load shaker model and to achieve the control objective. The controller was made by a finite impulse response (FIR) filter, were the weight are adaptively updated in real time. A training mode was used in order to define a starting point for the filter coefficients, and a limited bandwidth noise was used to stimulate the plant. This method of using a training mode at the system start-up results useful in different aspects. First, a non-model based approach (model-free), allows to design a controller directly without pre identification of the shaker model, witch means a lower computational complexity. Second, it reduces the mean squared error (MSE) when the real experiment starts, and allows to have a relatively small MSE during the all experiments.
The identification of the shaker model, by using the time domain adaptive filter algorithm such as Least Mean Square (LMS) criteria, is the best method to overcome identification instability [46]. However, this method has a drawbacks, because it required hundreds if not thousands of adaptive weights to effectively represent a high order system like an electrodynamic shaker and the specimen. Coefficients adaptation involve intensive computations and large memory to store the weights.

Besides, even the training mode reduce considerably the problem, the time domain algorithm is input dependent, and the convergence rate is influenced by the input covariance matrix eigenvalue spread.
To overcome the drawback of the time domain adaptive filter, a frequency domain adaptive algorithm could be used as alternatives in future research. The frequency domain adaptive filter algorithm (FDAF), such as block adaptive filtering method, has superior proprieties in terms of convergence rate and computational resources, with respect to the time domain method [34]. However it has the drawback of a long time-delay because it utilise block processing, and it could be a problem in real time application.

Bibliography

[1] M. P. Peter Spies, Loreto Mateu, *Handbook of Energy Harvesting Power Supplies and Applications*. Pan Stanford Publishing Pte Ltd, 2012. [Online]. Available: http://www.ebook.de/de/product/13048192/handbook_of_energy_harvesting_power_supplies_and_applications.html

[2] M. Ferrari, V. Ferrari, M. Guizzetti, and D. Marioli, "An autonomous battery-less sensor module powered by piezoelectric energy harvesting with rf transmission of multiple measurement signals," *Smart Materials and Structures*, vol. 18, no. 8, p. 085023, 2009.

[3] *Advances in Energy Harvesting Methods*. Springer-Verlag GmbH, 2013. [Online]. Available: http://www.ebook.de/de/product/19453833/advances_in_energy_harvesting_methods.html

[4] Y. Uchiyama and M. Fujita, "Robust acceleration and displacement control of electrodynamic shaker," in *Computer Aided Control System Design, 2006 IEEE International Conference on Control Applications, 2006 IEEE International Symposium on Intelligent Control, 2006 IEEE*. IEEE, 2006, pp. 746–751.

[5] "Tira gmbh - vibration test system tv 52110."

[6] G. F. Lang and D. Snyder, "Understanding the physics of electrodynamic shaker performance," *Sound and Vibration*, vol. 35, no. 10, pp. 24–33, 2001.

[7] G. F. Lang, "Electrodynamic shaker fundamentals," *Sound and vibration*, vol. 31, no. 4, pp. 14–23, 1997.

[8] J. T. Broch, "Vibration exciter characteristics," Brüel & Kjær Sound & Vibration Measurement, Tech. Rep., 1960.

[9] F. Beltran-Carbajal, Ed., *Vibration Analysis and Control - New Trends and Developments*. InTech, sep 2011. [Online]. Available: http://dx.doi.org/10.5772/924

[10] B. Farhang-Boroujeny, *Adaptive filters: theory and applications*. John Wiley & Sons, 2013.

[11] J. Shynk, "Adaptive IIR filtering," *IEEE ASSP Magazine*, vol. 6, no. 2, pp. 4–21, apr 1989. [Online]. Available: http://dx.doi.org/10.1109/53.29644

[12] ——, "A complex adaptive algorithm for IIR filtering," *IEEE Transactions on Acoustics, Speech, and Signal Processing*, vol. 34, no. 5, pp. 1342–1344, oct 1986. [Online]. Available: http://dx.doi.org/10.1109/TASSP.1986.1164936

[13] M. Abe and M. Kawamata, "Comparison of the convergence of IIR evolutionary digital filters and other adaptive digital filters on a multiple-peak surface," in *Conference Record of the Thirty-First Asilomar Conference on Signals, Systems and Computers (Cat. No.97CB36136)*. Institute of Electrical & Electronics Engineers (IEEE). [Online]. Available: http://dx.doi.org/10.1109/ACSSC.1997.679187

[14] K. Thomas, H. Sayed Ali, and H. Babak, "Linear estimation," 2000.

[15] B. Widrow and S. D. Stearns, "Adaptive signal processing," *Englewood Cliffs, NJ, Prentice-Hall, Inc., 1985, 491 p.*, vol. 1, 1985.

[16] B. Widrow and M. Bilello, "Adaptive inverse control," in *Intelligent Control, 1993., Proceedings of the 1993 IEEE International Symposium on*, Aug. 1993, pp. 1–6.

[17] B. Widrow, J. McCool, and B. Medoff, "Adaptive control by inverse modeling," in *Twelfth Asilomar Conference on Circuits, Systems, and Computers*, 1978.

[18] E. W. Bernard Widrow, *Adaptive Inverse Control: A Signal Processing Approach*. JOHN WILEY & SONS INC, 2007. [Online]. Available: http://www.ebook.de/de/product/6732393/bernard_widrow_eugene_walach_adaptive_inverse_control_a_signal_processing_approach.html

[19] C. S. Ramalingam, "A note on the region of convergence of the z-transform," *Signal Processing*, vol. 88, no. 5, pp. 1297–1298, 2008.

[20] L. Inc., "Vibration testing products catalog and technical reference," Tech. Rep., Catalog 181.

[21] L. Della Flora and H. A. Grundling, "Time domain sinusoidal acceleration controller for an electrodynamic shaker," *Control Theory & Applications, IET*, vol. 2, no. 12, pp. 1044–1053, 2008.

[22] Y. Uchiyama, M. Mukai, and M. Fujita, "Robust acceleration control of electrodynamic shaker using μ -synthesis," in *Decision and Control, 2005 and 2005 European Control Conference. CDC-ECC '05. 44th IEEE Conference on*, 2005, pp. 6170–6175. [Online]. Available: http://ieeexplore.ieee.org/stamp/stamp.jsp?arnumber=1583149

[23] E. Sauther, "Sine sweep vibration testing for modal response primer."

[24] D. H. Herlufsen, Brüel&Kjær, "Modal analysis using multi-reference and multiple-input multiple-output techniques," Tech. Rep., 2012.

[25] D. O. Smallwood, "Characterizing electrodynamic shakers," Sandia National Labs., Albuquerque, NM (United States), Tech. Rep., 1996.

[26] PCB, "Accelerometer calibration report," Tech. Rep.

[27] C. Yager and C. Laber, "Switched-capacitor filters beat active filters at their own game," *TechOnLine. Disponível em¡ http://www. techonline. com/community/home/7534¿. Acesso em*, vol. 30, no. 07, 2006.

[28] http://www.icetlab.com/Documents/DS1104InstConfig.pdf.

[29] http://flyingv.ucsd.edu/azad/dSPACE˙tutorial.pdf.

[30] http://www.eleceng.ohiostate. edu/ passino/dSPACEtutorial.doc.pdf.

[31] J. G. Proakis, *Digital Communications*. McGraw-Hill Education Ltd, 2008. [Online]. Available: http://www.ebook.de/de/product/6965296/john_g_proakis_digital_communications.html

[32] R. W. Lucky, "Automatic equalization for digital communication," *Bell System Technical Journal*, vol. 44, no. 4, pp. 547–588, 1965.

[33] M. Sondhi, "An adaptive echo canceller," *Bell System Technical Journal*, vol. 46, no. 3, pp. 497–511, 1967.

[34] B. F.-B. Behrouz Farhang-Boroujeny, *Adaptive Filters: Theory and Applications*. JOHN WILEY & SONS INC, 2013. [Online]. Available: http://www.ebook.de/de/product/20823840/behrouz_farhang_boroujeny_b_farhang_boroujeny_adaptive_filters_theory_and_applications.html

[35] S. M. Kuo and D. Morgan, *Active noise control systems: algorithms and DSP implementations*. John Wiley & Sons, Inc., 1995.

[36] S. M. Kuo and D. R. Morgan, "Active noise control: a tutorial review," *Proceedings of the IEEE*, vol. 87, no. 6, pp. 943–973, Jun. 1999.

[37] B. Widrow and E. Walach, "The adaptive inverse control concept," in *IEEE Press Series on Power Engineering*. Wiley-Blackwell, pp. 1–39. [Online]. Available: http://dx.doi.org/10.1002/9780470231616.ch1

[38] V. Vandoren, *Techniques for Adaptive Control*. BUTTERWORTH HEINEMANN, 2002. [Online]. Available: http://www.ebook.de/de/product/3671214/vance_vandoren_techniques_for_adaptive_control.html

[39] J.-T. Jeng and T.-T. Lee, "Nonlinear adaptive inverse control via the unified model neural network," in *Applications and Science of Computational Intelligence II*, K. L. Priddy, P. E. Keller, D. B. Fogel, and J. C. Bezdek, Eds. SPIE-Intl Soc Optical Eng, mar 1999. [Online]. Available: http://dx.doi.org/10.1117/12.342869

[40] J. Kim, C.-W. Lee, J.-K. Lee, J.-S. Hwang, and J.-H. Park, "Comparison of adaptive systems for noise reduction in speech," in *2006 Proceeding of the Thrity-Eighth Southeastern Symposium on System Theory*. Institute of Electrical & Electronics Engineers (IEEE). [Online]. Available: http://dx.doi.org/10.1109/SSST.2006.1619050

[41] J. B. Lawrie and I. D. Abrahams, "A brief historical perspective of the wiener–hopf technique," *Journal of Engineering Mathematics*, vol. 59, no. 4, pp. 351–358, 2007.

[42] http://cwww.ee.nctu.edu.tw/course/asp/ASP04.pdf.

[43] S. R. D. Paulo, "Adaptive filtering: algorithms and practical implementation," *The international series in Engineering and Computer Scienc*, 2008.

[44] "Vibration testing and human response," in *Vibration*. Informa UK Limited, sep 2006, pp. 635–716. [Online]. Available: http://dx.doi.org/10.1201/b18521-11

[45] W. G. Ali and S. W. Ibrahim, "Power analysis for piezoelectric energy harvester," 2012.

[46] M. O. A. Ajangnay, "Hybrid time-frequency domain adaptive filtering algorithm for electrodynamic shaker control," *J. Eng. Comput. Innov.*, vol. 2, no. 9, dec 2011. [Online]. Available: http://dx.doi.org/10.5897/JECI11.052

List of Figures